



CMS-EXO-18-007

CERN-EP-2018-289
2019/02/26

Search for long-lived particles decaying into displaced jets in proton-proton collisions at $\sqrt{s} = 13$ TeV

The CMS Collaboration^{*}

Abstract

A search for long-lived particles decaying into jets is presented. Data were collected with the CMS detector at the LHC from proton-proton collisions at a center-of-mass energy of 13 TeV in 2016, corresponding to an integrated luminosity of 35.9 fb^{-1} . The search examines the distinctive topology of displaced tracks and secondary vertices. The selected events are found to be consistent with standard model predictions. For a simplified model in which long-lived neutral particles are pair produced and decay to two jets, pair production cross sections larger than 0.2 fb are excluded at 95% confidence level for a long-lived particle mass larger than 1000 GeV and proper decay lengths between 3 and 130 mm. Several supersymmetry models with gauge-mediated supersymmetry breaking or R -parity violation, where pair-produced long-lived gluinos or top squarks decay to several final-state topologies containing displaced jets, are also tested. For these models, in the mass ranges above 200 GeV , gluino masses up to $2300\text{--}2400\text{ GeV}$ and top squark masses up to $1350\text{--}1600\text{ GeV}$ are excluded for proper decay lengths approximately between 10 and 100 mm. These are the most restrictive limits to date on these models.

Published in Physical Review D as doi:10.1103/PhysRevD.99.032011.

1 Introduction

A large number of extensions to the standard model (SM) predict the production of long-lived particles at the CERN LHC that can further decay into final states containing jets. The theoretical motivations are extremely rich [1]; examples include split supersymmetry (SUSY) [2–7], SUSY with weak R -parity violation (RPV) [8–11], SUSY with gauge-mediated supersymmetry breaking (GMSB) [12–14], “stealth SUSY” [15, 16], “Hidden Valley” models [17–19], baryogenesis triggered by weakly interacting massive particles (WIMPs) [20–22] and twin Higgs models [23–25].

In this paper, we search for long-lived particles decaying into jets, with each long-lived particle having a decay vertex displaced from the production vertex by up to 55 cm in the transverse plane. Events used in this analysis were collected with the CMS detector [26] at the LHC from proton-proton (pp) collisions at a center-of-mass energy of 13 TeV in 2016, corresponding to an integrated luminosity of 35.9 fb^{-1} . The analysis examines dijets formed by jets clustered from energy deposits in the calorimeters. For the displaced-jet signal, the tracks left by charged particles originating from the decay of a long-lived particle will usually exhibit large displacements with respect to the primary vertex, allowing the reconstruction of a secondary vertex within the associated dijet. The properties of the secondary vertex can be utilized to discriminate between the long-lived signatures and the SM backgrounds. Although the objects studied here are dijets, two separate displaced single jets can pass the selection criteria, even when each displaced vertex contains only one jet. A variety of models predict long-lived particles decaying into displaced jets and we test several of them, including SUSY models with GMSB or RPV, as will be discussed in detail in Section 3.

Results of searches for similar long-lived particle signatures at $\sqrt{s} = 8 \text{ TeV}$ have been reported by ATLAS [27, 28], CMS [29–31], and LHCb [32, 33]. The ATLAS Collaboration has reported on a search at $\sqrt{s} = 13 \text{ TeV}$, which includes a missing transverse momentum requirement [34]. The CMS Collaboration has reported several long-lived particle searches at $\sqrt{s} = 13 \text{ TeV}$; one doesn’t utilize secondary vertex information [35], and another searches for a pair of displaced vertices within the beam pipe [36]. The search presented in this paper is designed to be sensitive to multiple final-state topologies containing displaced jets, and is therefore sensitive to a wide range of long-lived particle signatures.

2 The CMS detector

The central feature of the CMS apparatus is a superconducting solenoid of 6 m internal diameter, providing a magnetic field of 3.8 T. Within the solenoid volume are a silicon pixel and strip tracker, a lead tungstate crystal electromagnetic calorimeter (ECAL), and a brass and scintillator hadron calorimeter (HCAL), each composed of a barrel and two endcap detectors. Muons are detected in gas-ionization chambers embedded in the steel flux-return yoke outside the solenoid.

The silicon tracker measures charged particles in the pseudorapidity range $|\eta| < 2.5$. It consists of 1440 silicon pixel and 15 148 silicon strip detector modules. For nonisolated particles of $1 < p_T < 10 \text{ GeV}$ and $|\eta| < 1.4$, the track resolutions are typically 1.5% in p_T , and 25–90 (45–150) μm in the transverse (longitudinal) impact parameter [37].

In the region $|\eta| < 1.74$, the HCAL cells have widths of 0.087 in pseudorapidity and 0.087 in azimuth. In the η - ϕ plane, and for $|\eta| < 1.48$, the HCAL cells map on to 5×5 arrays of ECAL crystals to form calorimeter towers projecting radially outward from the nominal interaction

point. For $|\eta| > 1.74$, the coverage of the towers increases progressively to a maximum of 0.174 in $\Delta\eta$ and $\Delta\phi$. Within each tower, the energy deposits in ECAL and HCAL cells are summed to define the calorimeter tower energies, and are subsequently used to provide the energies and directions of hadronic jets.

Events of interest are selected using a two-tiered trigger system [38]. The first level (L1), composed of custom hardware processors, uses information from the calorimeters and muon detectors to select events at a rate of around 100 kHz within a time interval of less than $4\ \mu\text{s}$. The second level, known as the high-level trigger (HLT), consists of a farm of processors running a version of the full event reconstruction software optimized for fast processing, and reduces the event rate to around 1 kHz before data storage.

A more detailed description of the CMS detector, together with a definition of the coordinate system used and the relevant kinematic variables, can be found in Ref. [26].

3 Data sets and simulated samples

Data were collected with a dedicated HLT displaced-jet trigger. At the trigger level, jets are reconstructed from the energy deposits in the calorimeter towers, clustered using the anti- k_{T} algorithm [39, 40] with a distance parameter of 0.4. In this process, the contribution from each calorimeter tower is assigned a momentum, the absolute value and the direction of which are given by the energy measured in the tower and the coordinates of the tower. The raw jet energy is obtained from the sum of the tower energies, and the raw jet momentum from the vector sum of the tower momenta, which results in a nonzero jet mass. The raw jet energies are then corrected [41] to establish a relative uniform response of the calorimeter in η and a calibrated absolute response in transverse momentum p_{T} .

Events may contain multiple primary vertices, corresponding to multiple pp collisions occurring in the same bunch crossing. The reconstructed vertex with the largest value of summed physics-object p_{T}^2 is taken to be the primary pp interaction vertex, referred to as the leading primary vertex. The physics objects are the “jets,” clustered using the jet finding algorithm [39, 40] with the tracks assigned to the vertex as inputs, and the associated missing transverse momentum, taken as the negative vector sum of the p_{T} of those jets. More details are given in Section 9.4.1 of Ref. [42].

The displaced-jet trigger requires an H_{T} larger than 350 GeV, where H_{T} is defined as the scalar sum of the transverse momenta of all jets satisfying $p_{\text{T}} > 40\ \text{GeV}$ and $|\eta| < 2.5$ in the event. The trigger also requires the presence of at least two jets, each of them satisfying the following requirements:

- $p_{\text{T}} > 40\ \text{GeV}$ and $|\eta| < 2.0$;
- at most two associated prompt tracks, which are tracks having a transverse impact parameter (with respect to the leading primary vertex) smaller than 1.0 mm; and
- at least one associated displaced track, defined as a track with a transverse impact parameter (with respect to the leading primary vertex) larger than 0.5 mm, and an impact parameter significance larger than 5.0, where the significance is the ratio of the impact parameter to its uncertainty.

The main background of this analysis arises from the SM events comprised uniquely of jets produced through the strong interaction, referred to as quantum chromodynamics (QCD) multijet events. The QCD multijet sample is simulated with MADGRAPH5_aMC@NLO 2.2.2 [43] at lead-

ing order, which is interfaced with PYTHIA 8.212 [44] for parton showering, hadronization, and fragmentation. Jets from the matrix element calculations are matched to parton shower jets using the MLM algorithm [45]. The CUETP8M1 tune [46] is used for modeling the underlying event. For parton distribution function (PDF) modeling, the NNPDF3.0 PDF set [47] is used.

One of the benchmark signal models is a simplified model, referred to as the jet-jet model, where long-lived scalar neutral particles X are pair-produced through a $2 \rightarrow 2$ scattering process, mediated by an off-shell Z boson propagator. Each X particle decays to a quark-antiquark pair, and is assumed to do so with equal branching fractions to u , d , s , c , and b quark pairs. Although X could decay to top quark pairs, we chose a signature with a simple topology, such that the analysis strategy would be sensitive to a variety of models. Simulation shows that exclusion of the top quark pair decay mode leads to only small changes in the signal efficiency. The chosen signature has two displaced vertices, each of them the origin of one displaced jet pair. The samples are produced with different resonance masses ranging from 50 to 3000 GeV, and with different proper decay lengths ranging from 1 mm to 10 m.

Several SUSY models with long-lived particles are considered, where we mainly focus on testing SUSY particles with masses larger than 200 GeV. The first is a GMSB SUSY model [1], in which the gluino is long lived and then decays to a gluon and a gravitino, referred to as the $\tilde{g} \rightarrow g\tilde{G}$ model. The gravitino is assumed to be the lightest supersymmetric particle (LSP) and manifests itself as missing transverse momentum. The signature is two displaced vertices, each of them the origin of a single displaced jet and missing transverse momentum. The samples are produced with gluino masses from 800 to 2500 GeV, and a proper decay length varying from 1 mm to 10 m.

The second is an RPV SUSY model [48] with minimum flavor violation, where the gluino is long lived and decays to a top quark and a top squark, the top squark is assumed to be virtual and decays to a strange antiquark and a bottom antiquark through the RPV interaction with strength given by the coupling λ''_{323} [11], effectively resulting in a three-body decay with a “multijet” final-state topology. This model is referred to as the $\tilde{g} \rightarrow tbs$ model. The samples are produced with gluino masses from 1200 to 3000 GeV, and a proper decay length varying from 1 mm to 10 m.

Other signal models considered include an RPV SUSY model [49], in which the long-lived top squark decays to a bottom quark and a charged lepton via RPV interactions with strengths given by couplings λ'_{331} , λ'_{332} , and λ'_{333} [11], assuming the decay rate to each of the three lepton flavors to be equal, referred to as the $\tilde{t} \rightarrow bl$ model. The samples are produced with different top squark masses from 200 to 1600 GeV, and a proper decay length varying from 1 mm to 1 m.

We also consider another SUSY model motivated by dynamical R -parity violation (dRPV) [50, 51], where the long-lived top squark decays to two down antiquarks via RPV interaction with strength given by a nonholomorphic RPV coupling η''_{311} [52], referred to as the $\tilde{t} \rightarrow \bar{d}\bar{d}$ model. The samples are produced with different top squark masses from 800 to 1800 GeV, and proper decay length varying from 1 mm to 10 m.

All signal samples are produced with PYTHIA 8.212, and NNPDF2.3QED [53] is used for PDF modeling. When a gluino or top squark is long lived, it will have enough time to form a hadronic state, an R -hadron [9, 54, 55], which is simulated with PYTHIA. For underlying event modeling the CUETP8M1 tune is utilized.

Both the background and the signal events are processed with a GEANT4-based [56] simulation for detailed CMS detector response. To take account of the effects of additional pp interactions within the same or nearby bunch crossings (“pileup”), additional minimum bias events are

overlaid on the simulated events to match the pileup distribution observed in the data.

4 Event reconstruction and preselection

The offline jet reconstruction and primary vertex selection follow the same procedures applied at the trigger level (as described in Section 3), except that the full offline information is used. After the trigger selection, events are selected offline requiring $H_T > 400 \text{ GeV}$; dijet candidates are formed from all possible pairs of jets in the event, where the jets are required to have transverse momenta $p_T > 50 \text{ GeV}$ and pseudorapidity $|\eta| < 2.0$. These selection criteria are chosen so that the online H_T and jet p_T requirements in the trigger are fully efficient. The track candidates used in this analysis are required to have “high purity” and to have transverse momenta $p_T > 1 \text{ GeV}$. The “high-purity” selection utilizes track information (including the normalized χ^2 of the track fit, the impact parameters, and the hits in different layers) to reduce the fake rate and is optimized separately for each iteration of the track reconstruction, so that it is efficient for selecting tracks with different displacements. More details of the “high-purity” selection can be found in Section 4.4 of Ref. [37]. The η and ϕ of the track are determined by the direction of the momentum vector at the closest point to the leading primary vertex. The tracks are then associated with the jets by requiring $\Delta R < 0.5$, where $\Delta R = \sqrt{(\Delta\eta)^2 + (\Delta\phi)^2}$ and $\Delta\eta$ ($\Delta\phi$) is the difference in η (ϕ) between the jet axis and the track direction. If a track satisfies $\Delta R < 0.5$ for more than one jet, it is associated with the jet with smaller ΔR .

To reconstruct secondary vertices, displaced tracks associated with each dijet candidate are selected by requiring transverse impact parameters (with respect to the leading primary vertex) larger than 0.5 mm and transverse impact parameter significances larger than 5 . An adaptive vertex fitter algorithm [57] is then used for reconstructing a possible secondary vertex (containing at least 2 tracks) with the displaced tracks in each dijet. The adaptive vertex fitter utilizes an annealing algorithm in which the outlier tracks are down-weighted for each step, and thus exhibits robustness against outlier tracks. Only secondary vertices with a χ^2 per degree-of-freedom (χ^2/n_{dof}) of less than 5.0 are selected. Also, the four-momentum of the vertex is reconstructed assuming the pion mass for all assigned tracks; the invariant mass of the vertex is required to be larger than 4 GeV , and the transverse momentum of the vertex is required to be larger than 8 GeV , in order to suppress long-lived SM mesons and baryons.

Each dijet candidate is required to have one reconstructed secondary vertex satisfying the above selection criteria. Furthermore, we select the track with the second-highest transverse (two-dimensional) impact parameter (IP) significance among the tracks that are assigned to the secondary vertex (the highest two-dimensional IP significance is usually more sensitive to the tail of impact parameter distribution in the background process, and is therefore less powerful). For displaced-jet signatures, where tracks tend to be more displaced, the two-dimensional IP significance of this selected track will be large. If it is smaller than 15 , the dijet candidate is rejected. We also compute the ratio between the sum of energy for all the tracks assigned to the secondary vertex and the sum of the energy for all the tracks associated with the two jets. This ratio is expected to be large for displaced-jet signatures, therefore dijet candidates with a ratio smaller than 0.15 are rejected.

An additional variable, ζ , is defined to characterize the contribution of prompt activity to the jets. For each track associated with a jet, the primary vertex (including the leading primary vertex and the pileup vertices) with the minimum three-dimensional impact parameter significance to the track is identified. If this minimum three-dimensional impact parameter significance is smaller than 5 , we assign the track to this primary vertex. Then for each jet, we

Table 1: Summary of the preselection criteria

Secondary-vertex/dijet variable	Requirement
Vertex $\chi^2/\text{n}_{\text{dof}}$	<5.0
Vertex invariant mass	>4 GeV
Vertex transverse momentum	>8 GeV
Second largest two-dimensional IP significance	>15
Vertex track energy fraction in the dijet	>0.15
ζ (charged energy fraction associated with compatible primary vertices)	<0.20

compute the track energy contribution from each primary vertex, and the primary vertex with the largest track energy contribution to the jet is chosen. Finally, we define ζ as

$$\zeta = \frac{\sum_{\text{track} \in \text{PV}_1} E_{\text{track}}^{\text{Jet}_1} + \sum_{\text{track} \in \text{PV}_2} E_{\text{track}}^{\text{Jet}_2}}{E_{\text{Jet}_1} + E_{\text{Jet}_2}}, \quad (1)$$

which is the charged energy fraction of the dijet associated with the most compatible primary vertices. For displaced-jet signatures, ζ tends to be small since the jets are not compatible with primary vertices. Dijet candidates with ζ larger than 0.2 are rejected.

We do not require the secondary vertex to contain tracks from both jets in the dijet candidate. Two displaced single jets originating from two separate displaced vertices can be paired together and pass the selection, thus the search can be sensitive to long-lived particles decaying to a single jet (as in the $\tilde{g} \rightarrow g\tilde{G}$ model).

The preselection criteria of the analysis are summarized in Table 1. The variables used in the preselection are checked in data and QCD multijet MC events, and are found to be well-modeled in the MC events.

5 Event selection and background prediction

In addition to the secondary vertex reconstruction based on the adaptive vertex fitter, an auxiliary algorithm is explored. For each displaced track (as defined in Section 3) associated with the dijet, an expected decay point consistent with the displaced dijet hypothesis is determined by finding the crossing point between the track helix and the dijet direction in the transverse plane. The displaced tracks associated with the dijet are then clustered based on the expected transverse decay length with respect to the leading primary vertex L_{xy}^{exp} using a hierarchical clustering algorithm [58], in which two clusters are merged together when the smallest expected transverse decay length difference between the two clusters is smaller than 15% of the transverse decay length (L_{xy}) of the secondary vertex. When more than one cluster is formed after the final step of the hierarchical clustering, the one closest to the secondary vertex is selected. The cluster root-mean-square (RMS), which is a relative RMS of individual tracks L_{xy}^{exp} with respect to the secondary vertex L_{xy} , is computed to provide signal-background discrimination:

$$\text{RMS}_{\text{cluster}} = \sqrt{\frac{1}{N_{\text{tracks}}} \sum_{i=1}^{N_{\text{tracks}}} \frac{(L_{xy}^{\text{exp}}(i) - L_{xy})^2}{L_{xy}^2}}. \quad (2)$$

We then construct a likelihood discriminant based on three variables:

- vertex track multiplicity;
- vertex L_{xy} significance;

- cluster RMS.

The three variables are chosen so that the correlations between them are small. The likelihood discriminant, \mathcal{L} , is defined as

$$\mathcal{L} = \frac{p_S}{p_S + p_B} = \frac{1}{1 + p_B/p_S} = \frac{1}{1 + \prod_i p_{Bi}/p_{Si}}, \quad (3)$$

where $p_S(p_B)$ is the probability distribution function of the signal (background), and i is the label for different variables. Simulated jet-jet model events and simulated QCD multijet events are used to derive the probability distribution functions, where jet-jet model events with $m_X = 300$ and 1000 GeV , and with $c\tau_0 = 1, 3, 10, 30, 100, 300$, and 1000 mm are added together to derive p_S . When building the likelihood discriminant the trigger requirement is removed, since the number of simulated events is limited. Figure 1 shows the distributions of the three variables used to build the likelihood discriminant, as well as the discriminant itself, with selections on H_T and jet kinematic variables applied. Simulated signal events for the jet-jet model with $m_X = 300\text{ GeV}$ at different proper decay lengths $c\tau_0$ are also shown for comparison.

Two other variables are utilized in the event selection. One is the number of three-dimensional prompt tracks in a single jet, where three-dimensional prompt tracks are the tracks with three-dimensional impact parameters (with respect to the leading primary vertex) smaller than 0.3 mm . The other is the jet energy fraction carried by two-dimensional prompt tracks, referred to as the charged prompt energy fraction, where two-dimensional prompt tracks are those having transverse impact parameters (with respect to the leading primary vertex) smaller than 0.5 mm .

If more than one dijet candidate passes the preselections described in Section 4, the one with the largest track multiplicity is selected. When the track multiplicities are the same, the one with the smallest χ^2 per degree-of-freedom is selected. The candidate is then required to pass three final selection criteria. The first makes a selection on the number of three-dimensional prompt tracks and on the charged prompt energy fraction for the leading jet, while the second places a similar requirement on the same variables for the subleading jet. The third makes a selection on the discriminant variable \mathcal{L} . The three selection criteria are chosen such that the correlations between them are small for background events. The numerical values of the selection criteria are chosen by optimizing the signal sensitivity for the jet-jet model across different proper decay lengths ($1\text{--}1000\text{ mm}$) and different X masses ($100\text{--}1000\text{ GeV}$). The final selection criteria are determined to be

- Selection 1: for the leading jet in the dijet candidate, the number of three-dimensional prompt tracks is smaller than 2, the charged prompt energy fraction is smaller than 15%;
- Selection 2: for the subleading jet in the dijet candidate, the number of three-dimensional prompt tracks is smaller than 2, the charged prompt energy fraction is smaller than 13%; and
- Selection 3: \mathcal{L} is larger than 0.9993.

For the jet-jet model, when $m_X = 1000\text{ GeV}$ and after all the selection criteria are applied, the signal efficiencies for proper decay lengths $c\tau_0 = 1, 10, 100$, and 1000 mm are 9.7, 57, 45, and 7.8%, respectively. When $m_X = 100\text{ GeV}$, the signal efficiencies for $c\tau_0 = 1, 10, 100$ and, 1000 mm are 0.9, 4.4, 1.6, and 0.2%, respectively. More details of the signal efficiencies for different signal models can be found in Tables 6–10 of Appendix A.

Based on the three selections above, eight nonoverlapping regions are defined (regions A–H), as shown in Table 2. The signal region (region H) is defined for events passing all three

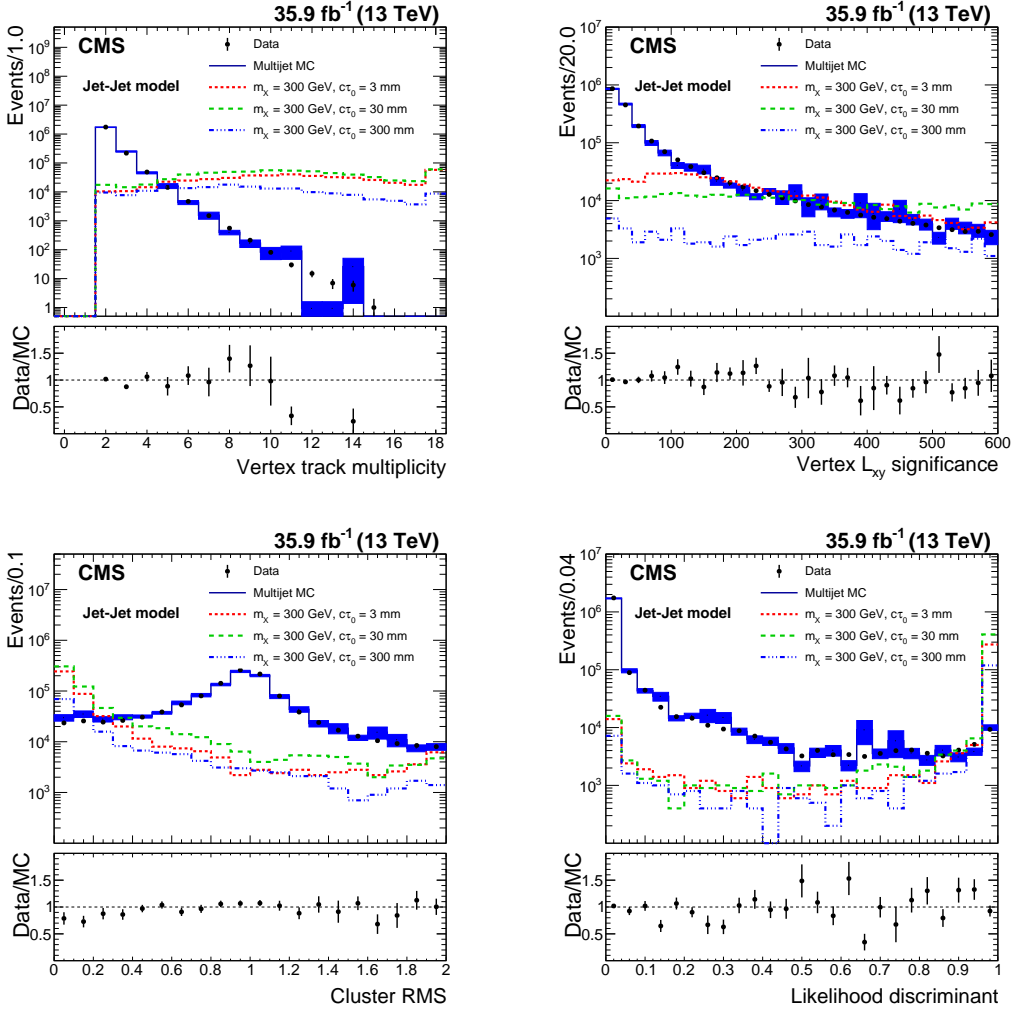


Figure 1: The distributions of vertex track multiplicity (upper left), vertex L_{xy} significance (upper right), cluster RMS (lower left), and likelihood discriminant (lower right), for data, simulated QCD multijet events, and simulated signal events. The lower panel of each plot shows the ratio between the data and the simulated QCD multijet events. Data and simulated events are selected with the displaced-jet trigger. The offline H_T is required to be larger than 400 GeV, and the jets are required to have $p_T > 50 \text{ GeV}$ and $|\eta| < 2.0$. The error bars and bands represent the statistical uncertainties of each distribution. Three benchmark signal distributions are shown (dashed lines) for the jet-jet model with $m_X = 300 \text{ GeV}$ and varying lifetimes. For visualization each signal process is given a cross section, σ , such that $\sigma 35.9 \text{ fb}^{-1} = 1 \times 10^6$.

Table 2: The definition of the different regions used in the background estimation.

Region	Selection 1	Selection 2	Selection 3
A	Fail	Fail	Fail
B	Pass	Fail	Fail
C	Fail	Pass	Fail
D	Fail	Fail	Pass
E	Fail	Pass	Pass
F	Pass	Fail	Pass
G	Pass	Pass	Fail
H	Pass	Pass	Pass

selections. The rest of the regions (A–G) are when events fail one or more of the three selections. The background estimate relies on the three selection criteria having little correlation between them. The background yield in the signal region H is predicted by different ratios of event counts in regions A–G, where the ratio $G(D+E+F)/(A+B+C)$ uses the fraction of events passing to those failing the likelihood discriminant selection (selection 3) and is taken as the central value of the predicted background events. Three additional ratios are evaluated using the events failing one or both of the other two selections (selections 1 and 2):

- cross-check 1: $G(D+E)/(A+C)$, uses events that fail selection 1;
- cross-check 2: $G(D+F)/(A+B)$, uses events that fail selection 2; and
- cross-check 3: $G(E+F)/(B+C)$, uses events that fail either selection 1 or selection 2.

These cross-checks provide an important test of the robustness of the background prediction and the assumption that the three selection criteria are minimally correlated. Differences between the predictions obtained with the nominal method and the cross-checks are also used to estimate the systematic uncertainty in the background prediction.

The nominal background prediction and the cross-checks are first tested with simulated QCD multijet events, and are found to be robust against different numerical values for the selection criteria. The method is also checked in data by using a control region defined to be independent to the signal region. This is achieved by inverting the selection on the vertex track energy fraction in the dijet, requiring this fraction to be less than 0.15. In addition, in order to improve the statistical precision in the control region, the following two requirements are relaxed relative to the baseline selection:

- number of three-dimensional prompt tracks smaller than 4; and
- charged prompt energy fraction smaller than 0.4.

The nominal background prediction and cross-checks are then tested in the control region for different threshold values of the likelihood discriminant. The numbers of predicted and observed background events for the nominal background method and the three cross-checks in the control region are summarized in Fig. 2 and Table 3. The p -value of each observation is computed based on the lower-tail of a Poisson distribution convolved with a normalized Gaussian function for statistical and systematic uncertainties. The p -value is then converted to a Z-value using the error function,

$$Z = \sqrt{2} \operatorname{erf}^{-1}[2p - 1], \quad (4)$$

which represents the observed significance, expressed as an equivalent number of standard deviations. The Z-values are also listed in the Table 3 for different threshold values of the likelihood discriminant, where the magnitudes of the Z-values are smaller than 1.5 standard

deviations.

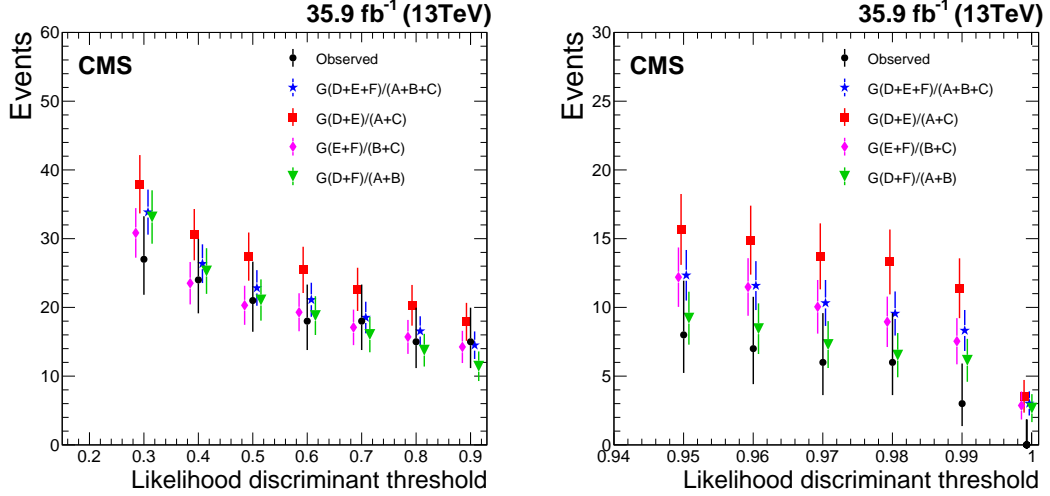


Figure 2: Numbers of predicted and observed background events for the nominal background method and the three cross-checks in the control region. Shown are the comparisons for likelihood discriminant thresholds of 0.3, 0.4, 0.5, 0.6, 0.7, 0.8, and 0.9 (left); and for thresholds of 0.95, 0.96, 0.97, 0.98, 0.99, and 0.9993 (right). The error bars represent the statistical uncertainties of the predictions and the observations. The data points at different likelihood discriminant thresholds are correlated, since the events passing higher likelihood discriminant thresholds also pass lower likelihood discriminant thresholds.

Table 3: The predicted and observed background in the control region for different likelihood discriminant thresholds. The background predictions are shown together with their statistical (first) and systematic (second) uncertainties (the systematic uncertainties in the background predictions are described in Section 6). The observed significances are also shown in terms of Z-values, and are smaller than 1.5 standard deviations.

Discriminant threshold	Predicted background	Observed background	Z-value
0.3	$33.9 \pm 3.3 \pm 4.1$	27	-0.80
0.5	$22.8 \pm 2.6 \pm 4.6$	21	-0.14
0.7	$18.5 \pm 2.3 \pm 4.1$	18	0.05
0.9	$14.5 \pm 2.0 \pm 3.4$	15	0.24
0.99	$8.3 \pm 1.5 \pm 3.1$	3	-1.12
0.9993	$3.0 \pm 0.9 \pm 0.5$	0	-1.40

6 Systematic uncertainties

The systematic uncertainties considered include the uncertainty in the background prediction, and the uncertainties in the signal yields. The integrated luminosity uncertainty for the 2016 13 TeV pp collision data recorded by the CMS detector is determined to be 2.5% [59], and is applied as a systematic uncertainty in the signal yields.

The systematic uncertainty in the background prediction is taken to be the largest deviation from the nominal background prediction ($G(D+E+F)/(A+B+C)$) to the three cross-checks described in Section 5, and is found to be 11% for the background yields in the signal region.

The signal efficiencies are calculated with simulated signal samples. The uncertainty in the efficiency of the online H_T requirement for the trigger emulation is determined by measuring

the efficiency with the events collected with an isolated single-muon trigger. The deviation from full efficiency as a function of offline H_T for events above the offline H_T threshold is taken as a correction and applied to the signal samples. Half of each of the corrections for the signal yields are taken as systematic uncertainties, and are calculated for different masses and proper decay lengths. The largest correction is 5%, thus a systematic uncertainty of 2.5% is assigned for all the signal points.

The uncertainty in the efficiency of the online jet p_T requirement is obtained by comparing the per-jet efficiency measured using the data collected with a prescaled H_T trigger that requires $H_T > 325\text{ GeV}$, with the efficiency determined from simulated multijet events. Above the offline p_T threshold, both efficiencies are close to 100%, and the difference between them is negligible, thus no corresponding systematic uncertainty is assigned.

Similarly, the uncertainty in the efficiency of the online tracking requirement for the trigger emulation is obtained by comparing the per-jet efficiency measured using the data collected with the prescaled H_T trigger with the efficiency determined from simulated multijet events. The differences in the efficiencies between data and simulation are parameterized as functions of the number of offline prompt and displaced tracks, where the convention of “prompt” and “displaced” follows the same definitions described in Section 3. The difference in the efficiencies is treated as a bias for the probability of a single jet passing the online tracking requirement, and is applied to the simulated signal samples. The systematic uncertainty is then determined by computing the variation of the efficiency for signal events to have at least two jets passing the online tracking requirement. The largest variation is 9%–10% for the considered signal models in the studied mass-lifetime range, which is taken as the corresponding systematic uncertainty.

To estimate the uncertainty in the offline vertex reconstruction, the events selected with the prescaled H_T trigger are utilized, from which dijet candidates are reconstructed using the same vertex reconstruction procedure and the same jet kinematics selections as in the offline analysis. We then compare the data with simulated multijet events in the secondary vertex transverse decay length and vertex track multiplicity distributions. We find that the main inconsistency between data and multijet simulation lies in the vertex track multiplicity. A reweighting factor is therefore extracted as a function of the number of tracks in the secondary vertex, and is interpreted as the correction for the vertex survival probabilities. The correction is then applied to simulated signal samples vertex-by-vertex, and the systematic uncertainty is obtained by computing the variations of signal efficiencies after the correction. The uncertainty is found to be 2%–15% for different signal models in the tested mass-lifetime range.

The uncertainty in the track reconstruction is estimated by studying the track impact parameter measurement in the data and in the multijet simulation, using the events selected with the prescaled H_T trigger. The possible mismodeling of the impact parameters is taken into account by varying the impact parameters in the signal samples by the same magnitude. The largest variation in the signal efficiency is taken as the corresponding uncertainty, and is found to be 14%–20% for different signal models.

The jet energy scale uncertainty is obtained by varying the jet energy correction [41] by one standard deviation. The resulting uncertainty is 2%–4% for the considered signal models.

The uncertainty in the choice of PDF sets is estimated by reweighting the signal events using NNPDF3.0, CT14 [60] and MMHT14 [61] PDF sets, and their associated uncertainty sets [62, 63]. The uncertainty in signal efficiencies is quantified by comparing the efficiencies calculated with alternative PDF sets and the ones with the nominal NNPDF set, and is found to be 4%–6% for the considered signal models.

The uncertainty in the selection of the primary vertex is estimated by replacing the leading primary vertex with the subleading vertex when calculating impact parameters and vertex displacement, where the primary vertices are ordered based on their values of summed physics-object p_T^2 as described in Section 3. The resulting uncertainty in signal efficiency is found to be 6%–15% for different signal models in the tested mass-lifetime range.

A summary of different sources of systematic uncertainties in the signal yields can be found in Table 4. For each signal model, the largest variations due to each source across the tested mass-lifetime points are taken as the corresponding systematic uncertainties.

Table 4: Systematic uncertainties in the signal yields, for each signal model studied. The quoted values reflect the largest variations due to each source for each signal model, in the studied range of masses and proper decay lengths.

Source	Jet-jet model	$\tilde{g} \rightarrow g\tilde{G}$	$\tilde{g} \rightarrow tbs$	$\tilde{t} \rightarrow b\ell$	$\tilde{t} \rightarrow \bar{d}\bar{d}$
Integrated luminosity	2.5%	2.5%	2.5%	2.5%	2.5%
Online H_T requirement	2.5%	2.5%	2.5%	2.5%	2.5%
Online tracking requirement	9%	9%	9%	9%	10%
Offline vertexing	15%	2%	6%	5%	2%
Track impact parameter modeling	14%	16%	20%	10%	20%
Jet energy scale	4%	2%	2%	2%	2%
PDF	5%	6%	4%	5%	4%
Primary vertex selection	6%	10%	15%	8%	12%
Total	24%	22%	28%	18%	26%

7 Results

7.1 Data in the signal region

We divide the signal region in bins of H_T and the number of dijets passing the preselection criteria in order to gain sensitivity to long-lived particles with different masses. After applying all the selection criteria described in Sections 4 and 5, we observe one event in the data, in accord with the total background prediction of 1.03 ± 0.19 (stat) ± 0.11 (syst) events. This observed event has an H_T of 590 GeV; and yields a secondary vertex candidate, with a transverse decay length of 3.5 cm and a track multiplicity of 10. This is consistent with the presence of a b quark jet, where the bottom hadron travels in the tracker for an extremely long distance before it decays.

Table 5 shows the predicted background and observations in the different bins of the signal region, where the sum of the predicted background in the four bins is consistent with the total background prediction quoted earlier. We find the observed yield is consistent with the predicted background in all bins, and we use the results in the four bins to set limits on a variety of models.

7.2 Interpretation of results

We set upper limits on the production cross section versus mass or lifetime for a given model by computing the 95% confidence level (CL) associated with each signal point according to the CL_s prescription [64–67], using an LHC-style profile likelihood ratio [66, 67] as the test statistics. The CL_s values are calculated using the asymptotic approximation [66], and are verified with full-frequentist results for representative signal points. The signal yields in the four bins in

Table 5: Summary of predicted and observed events in the signal region, for different H_T and number of dijet candidates values.

Selection on H_T	Number of dijets	Expected	Observed
$400 < H_T < 450 \text{ GeV}$	1	$0.42 \pm 0.14 \text{ (stat)} \pm 0.01 \text{ (syst)}$	0
$450 < H_T < 550 \text{ GeV}$	1	$0.23 \pm 0.08 \text{ (stat)} \pm 0.07 \text{ (syst)}$	0
$H_T > 550 \text{ GeV}$	1	$0.19 \pm 0.07 \text{ (stat)} \pm 0.05 \text{ (syst)}$	1
—	>1	$0.16 \pm 0.11 \text{ (stat)} \pm 0.06 \text{ (syst)}$	0

Table 5 are utilized to compute the CL_s values, and the systematic uncertainties are taken to be fully correlated across the four bins. The bin where more than one dijet candidate passes the preselection criteria usually brings most of the sensitivity in a given model since it often has the largest signal efficiency.

Figure 3 presents the expected and observed upper limits (at 95% CL) on the pair production cross section for the jet-jet model at different scalar particle X masses and proper decay lengths, assuming a 100% branching fraction. The limits are most stringent for $c\tau_0$ between 3 and 100 mm. For smaller decay lengths, the limits become less restrictive because of the vetoes on prompt activity. Since the tracking efficiency decreases with larger displacement, the limits also become less stringent for larger decay lengths when $c\tau_0 > 100$ mm. Pair production cross sections larger than 0.2 fb are excluded at high mass ($m_X > 1000$ GeV) for proper decay lengths between 3 and 130 mm. The lowest pair production cross section excluded is 0.13 fb, at $c\tau_0 = 30$ mm and long-lived particle mass $m_X > 1000$ GeV.

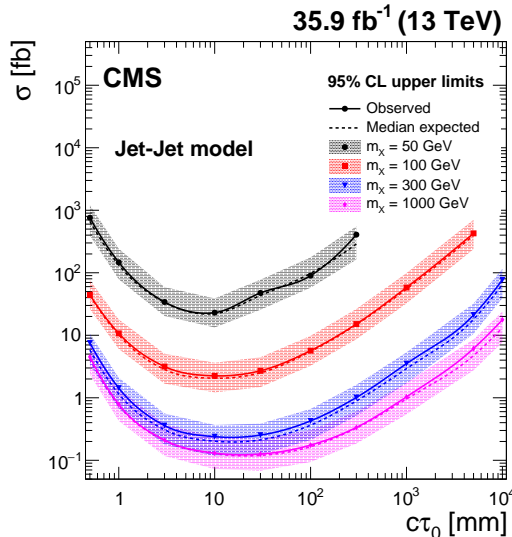


Figure 3: The expected and observed 95% CL upper limits on the pair production cross section of the long-lived particle X, assuming a 100% branching fraction for X to decay to a quark-antiquark pair, shown at different particle X masses and proper decay lengths for the jet-jet model. The solid (dashed) lines represent the observed (median expected) limits. The shaded bands represent the regions containing 68% of the distributions of the expected limits under the background-only hypothesis.

Figure 4 presents the expected and observed upper limits on the pair production cross section of long-lived gluino in the GMSB $\tilde{g} \rightarrow g\tilde{G}$ model, assuming a 100% branching fraction for the gluino to decay into a gluon and a gravitino. Although in the $\tilde{g} \rightarrow g\tilde{G}$ signature each displaced vertex is associated with only one jet, the two separate displaced single jets can be

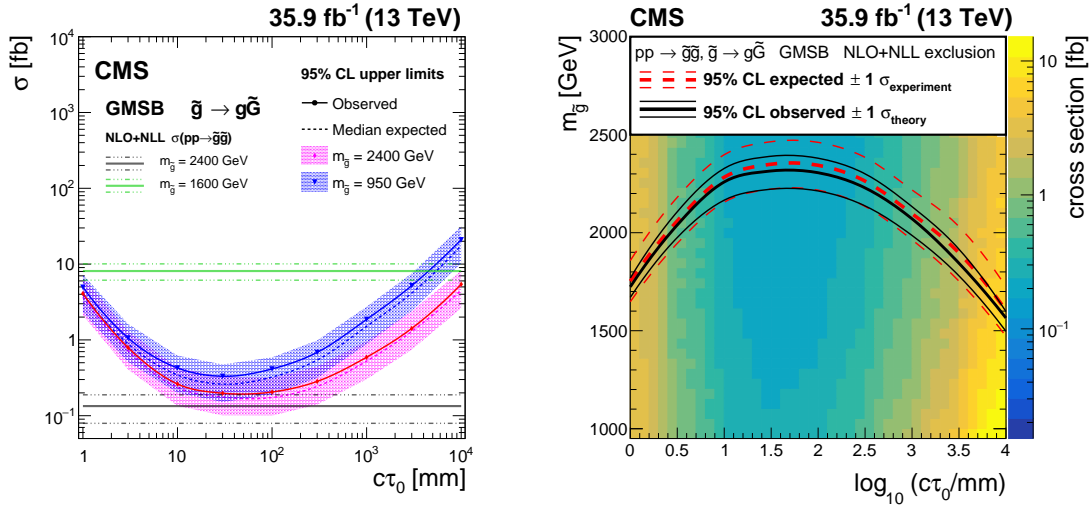


Figure 4: Left: the expected and observed 95% CL upper limits on the pair production cross section of the long-lived gluino, assuming a 100% branching fraction for $\tilde{g} \rightarrow g\tilde{G}$ decays. The horizontal lines indicate the NLO+NLL gluino pair production cross sections for $m_{\tilde{g}} = 2400 \text{ GeV}$ and $m_{\tilde{g}} = 1600 \text{ GeV}$, as well as their variations due to the uncertainties in the choices of renormalization scales, factorization scales, and PDF sets. The solid (dashed) lines represent the observed (median expected) limits, the bands show the regions containing 68% of the distributions of the expected limits under the background-only hypothesis. Right: the expected and observed 95% CL limits for the long-lived gluino model in the mass-lifetime plane, assuming a 100% branching fraction for $\tilde{g} \rightarrow g\tilde{G}$ decays, based on the NLO+NLL calculation of the gluino pair production cross section at $\sqrt{s} = 13 \text{ TeV}$. The thick solid black (dashed red) line represents the observed (median expected) limits at 95% CL. The thin black lines represent the change in the observed limit due to the variation of the signal cross sections within their theoretical uncertainties. The thin red lines indicate the region containing 68% of the distribution of the expected limits under the background-only hypothesis.

paired together and pass the selections, therefore the analysis is sensitive to this kind of signature. When the gluino mass is 2400 GeV, gluino pair production cross sections larger than 0.25 fb are excluded for proper decay lengths between 10 and 210 mm. When the proper decay length $c\tau_0 = 1 \text{ mm}$, the upper limit is insensitive to the gluino mass in the tested range since the signal acceptance is mainly limited by the online prompt track requirement in the displaced-jet trigger. The upper limits on the pair production cross section are then translated into upper limits on the gluino mass for different proper decay lengths, based on a calculation at the next-to-leading logarithmic accuracy matched to next-to-leading order predictions (NLO+NLL) of the gluino pair production cross section at $\sqrt{s} = 13 \text{ TeV}$ [68–72] in the limit where all the other SUSY particles are much heavier and decoupled. Gluino masses up to 2300 GeV are excluded for proper decay lengths between 20 and 110 mm. The bounds are the most stringent to date on this model in the tested proper decay length range.

Figure 5 presents the expected and observed upper limits on the pair production cross section of the long-lived gluino in the RPV $\tilde{g} \rightarrow t\bar{b}s$ model, assuming a 100% branching fraction for the gluino to decay to top, bottom, and strange antiquarks. The upper limits on the pair production cross section are translated into upper limits on the gluino mass for different proper decay lengths, based on the NLO+NLL calculation of the gluino pair production cross section at $\sqrt{s} = 13 \text{ TeV}$ [68–72] in the limit where all the other SUSY particles are much heavier and decoupled. Gluino masses up to 2400 GeV are excluded for proper decay lengths between 10 and 250 mm.

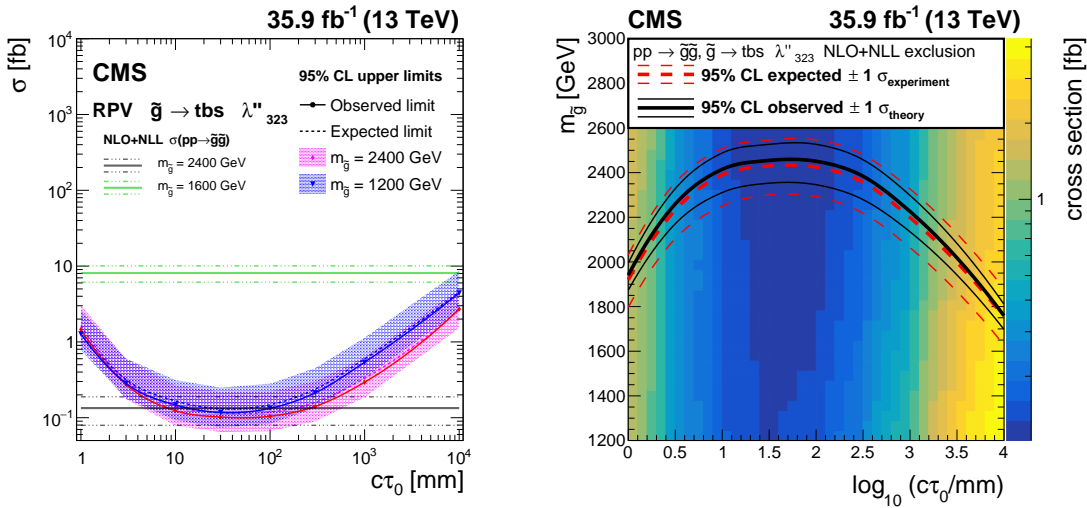


Figure 5: Left: the expected and observed 95% CL upper limits on the pair production cross section of the long-lived gluino, assuming a 100% branching fraction for $\tilde{g} \rightarrow \text{tbs}$ decays. The horizontal lines indicate the NLO+NLL gluino pair production cross sections for $m_{\tilde{g}} = 2400$ GeV and $m_{\tilde{g}} = 1600$ GeV, as well as their variations due to the uncertainties in the choices of renormalization scales, factorization scales, and PDF sets. The solid (dashed) lines represent the observed (median expected) limits, the bands show the regions containing 68% of the distributions of the expected limits under the background-only hypothesis. Right: the expected and observed 95% CL limits for the long-lived gluino model in the mass-lifetime plane, assuming a 100% branching fraction for $\tilde{g} \rightarrow \text{tbs}$ decays, based on the NLO+NLL calculation of the gluino pair production cross section at $\sqrt{s} = 13$ TeV. The thick solid black (dashed red) line represents the observed (median expected) limits at 95% CL. The thin black lines represent the change in the observed limit due to the variation of the signal cross sections within their theoretical uncertainties. The thin red lines indicate the region containing 68% of the distributions of the expected limits under the background-only hypothesis.

The bounds are currently the most stringent on this model for proper decay lengths between 10 mm and 10 m. A comparison on this model with the existing CMS search for displaced vertices within the beam pipe [36] can be found in Fig. 8 of Appendix A.

Figure 6 presents the expected and observed upper limits on the pair production cross section of the long-lived top squark in the RPV $\tilde{t} \rightarrow b\ell$ model, assuming a 100% branching fraction for the top squark to decay to a bottom quark and a charged lepton. The upper limits on the pair production cross section are then translated into upper limits on the top squark mass for different proper decay lengths, based on an NLO+NLL calculation of the top squark pair production cross section at $\sqrt{s} = 13$ TeV [68–72] in the limit where all the other SUSY particles are much heavier and decoupled. Top squark masses up to 1350 GeV are excluded for proper decay lengths between 7 and 110 mm. The bounds are currently the most stringent on this model for proper decay lengths between 3 mm and 1 m.

Figure 7 presents the expected and observed upper limits on the pair production cross section of the long-lived top squark in the dRPV $\tilde{t} \rightarrow dd$ model, assuming a 100% branching fraction for the top squark to decay to two down antiquarks. The upper limits on the pair production cross section are translated into upper limits on the top squark mass for different proper decay lengths assuming a 100% branching fraction, based on the NLO+NLL calculation of the top squark pair production cross section at $\sqrt{s} = 13$ TeV [68–72] in the limit where all the other SUSY particles are much heavier and decoupled. Top squark masses up to 1600 GeV are ex-

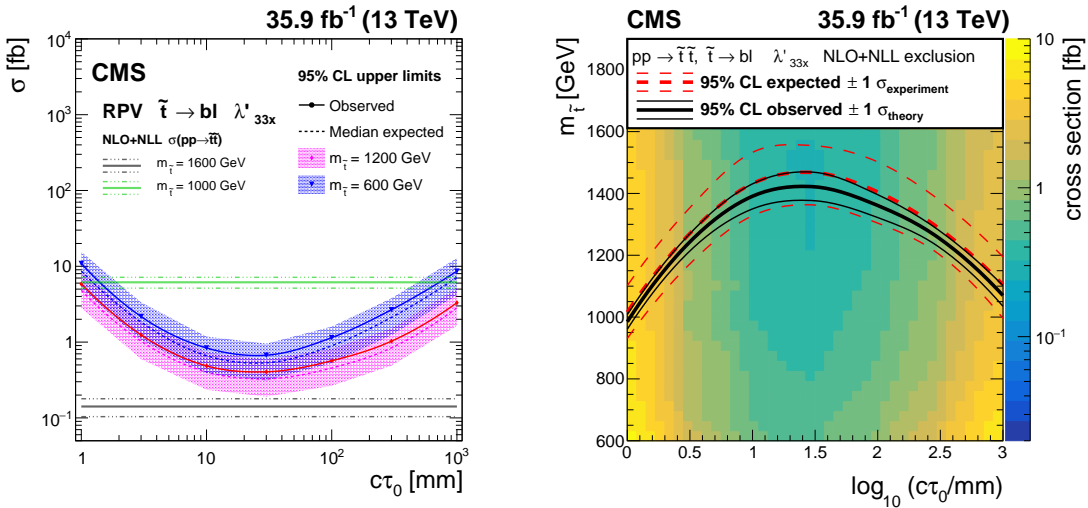


Figure 6: Left: the expected and observed 95% CL upper limits on the pair production cross section of the long-lived top squark, assuming a 100% branching fraction for $\tilde{t} \rightarrow b\ell$ decays. The horizontal lines indicate the NLO+NLL top squark pair production cross sections for $m_{\tilde{t}} = 1600$ GeV and $m_{\tilde{t}} = 1000$ GeV, as well as their variations due to the uncertainties in the choices of renormalization scales, factorization scales, and PDF sets. The solid (dashed) lines represent the observed (median expected) limits, the bands show the regions containing 68% of the distributions of the expected limits under the background-only hypothesis. Right: the expected and observed 95% limits for the long-lived top squark model in the mass-lifetime plane, assuming a 100% branching fraction for $\tilde{t} \rightarrow b\ell$ decays, based on the NLO+NLL calculation of the top squark pair production cross section at $\sqrt{s} = 13$ TeV. The thick solid black (dashed red) line represents the observed (median expected) limits at 95% CL. The thin black lines represent the change in the observed limit due to the variation of the signal cross sections within their theoretical uncertainties. The thin red lines indicate the region containing 68% of the distributions of the expected limits under the background-only hypothesis.

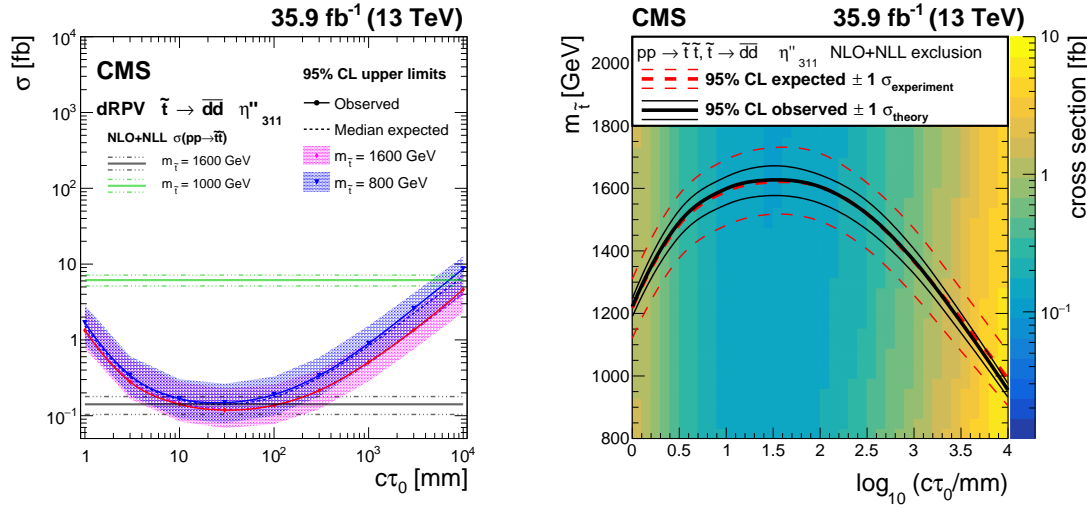


Figure 7: Left: the expected and observed 95% CL upper limits on the the pair production cross section of the long-lived top squark, assuming a 100% branching fraction for $\tilde{t} \rightarrow \bar{d}\bar{d}$ decays. The horizontal lines indicate the NLO+NLL top squark pair production cross sections for $m_{\tilde{t}} = 1600$ GeV and $m_{\tilde{t}} = 1000$ GeV, as well as their variations due to the uncertainties in the choices of renormalization scales, factorization scales, and PDF sets. The solid (dashed) lines represent the observed (median expected) limits, the bands show the regions containing 68% of the distributions of the expected limits under the background-only hypothesis. Right: the expected and observed 95% limits for the long-lived top squark model in the mass-lifetime plane, assuming a 100% branching fraction for $\tilde{t} \rightarrow \bar{d}\bar{d}$ decays, based on an NLO+NLL calculation of the top squark pair production cross section at $\sqrt{s} = 13$ TeV. The thick solid black (dashed red) line represents the observed (median expected) limits at 95% CL. The thin black lines represent the change in the observed limit due to the variation of the signal cross sections within their theoretical uncertainties. The thin red lines indicate the region containing 68% of the distribution of the expected limits under the background-only hypothesis.

cluded for proper decay lengths between 10 and 100 mm. The bounds are currently the most stringent on this model for proper decay lengths between 10 mm and 10 m. A comparison on this model with the existing CMS search for displaced vertices within the beam pipe [36] can be found in Fig. 8 of Appendix A.

8 Summary

A search for long-lived particles decaying to jets is presented, based on proton-proton collision data collected with the CMS experiment at a center-of-mass energy of 13 TeV in 2016, corresponding to an integrated luminosity of 35.9 fb^{-1} . The analysis utilizes a dedicated trigger to capture events with displaced-jet signatures, and exploits jet, track, and secondary vertex information to discriminate displaced-jet candidate events from those produced by the standard model and instrumental backgrounds. The observed yields in data are in agreement with the background predictions. For a variety of models, we set the best limits to date for long-lived particles with proper decay lengths approximately between 5 mm and 10 m. Upper limits are set at 95% confidence level on the pair production cross section of long-lived neutral particles decaying to two jets, for different masses and proper lifetimes, and are as low as 0.2 fb at high mass ($m_X > 1000$ GeV) for proper decay lengths between 3 and 130 mm. A supersymmetric (SUSY) model with gauge-mediated supersymmetry breaking (GMSB) is also tested, in which

the long-lived gluino can decay to one jet and a lightest SUSY particle. Upper limits are set on the pair production cross section of the gluino with different masses and proper decay lengths $c\tau_0$. Pair-produced long-lived gluinos lighter than 2300 GeV are excluded for proper decay lengths between 20 and 110 mm. For an R -parity violating (RPV) SUSY model, where the long-lived gluino can decay to top, bottom, and strange antiquarks, pair-produced gluinos lighter than 2400 GeV are excluded for decay lengths between 10 and 250 mm. For a second RPV SUSY model, in which the long-lived top squark can decay to one bottom quark and a charged lepton, pair-produced long-lived top squarks lighter than 1350 GeV are excluded for decay lengths between 7 and 110 mm. For another RPV SUSY model where the long-lived top squark decays to two down antiquarks, pair-produced long-lived top squarks lighter than 1600 GeV are excluded for decay lengths between 10 and 110 mm. These are the most stringent limits to date on these models.

Acknowledgments

We congratulate our colleagues in the CERN accelerator departments for the excellent performance of the LHC and thank the technical and administrative staffs at CERN and at other CMS institutes for their contributions to the success of the CMS effort. In addition, we gratefully acknowledge the computing centers and personnel of the Worldwide LHC Computing Grid for delivering so effectively the computing infrastructure essential to our analyses. Finally, we acknowledge the enduring support for the construction and operation of the LHC and the CMS detector provided by the following funding agencies: BMBWF and FWF (Austria); FNRS and FWO (Belgium); CNPq, CAPES, FAPERJ, FAPERGS, and FAPESP (Brazil); MES (Bulgaria); CERN; CAS, MoST, and NSFC (China); COLCIENCIAS (Colombia); MSES and CSF (Croatia); RPF (Cyprus); SENESCYT (Ecuador); MoER, ERC IUT, and ERDF (Estonia); Academy of Finland, MEC, and HIP (Finland); CEA and CNRS/IN2P3 (France); BMBF, DFG, and HGF (Germany); GSRT (Greece); NKFIA (Hungary); DAE and DST (India); IPM (Iran); SFI (Ireland); INFN (Italy); MS and NRF (Republic of Korea); MES (Latvia); LAS (Lithuania); MOE and UM (Malaysia); BUAP, CINVESTAV, CONACYT, LNS, SEP, and UASLP-FAI (Mexico); MOS (Montenegro); MBIE (New Zealand); PAEC (Pakistan); MSHE and NSC (Poland); FCT (Portugal); JINR (Dubna); MON, RosAtom, RAS, RFBR, and NRC KI (Russia); MESTD (Serbia); SEIDI, CPAN, PCTI, and FEDER (Spain); MOSTR (Sri Lanka); Swiss Funding Agencies (Switzerland); MST (Taipei); ThEPCenter, IPST, STAR, and NSTDA (Thailand); TUBITAK and TAEK (Turkey); NASU and SFFR (Ukraine); STFC (United Kingdom); Department of Energy and National Science Foundation (USA).

Individuals have received support from the Marie-Curie program and the European Research Council and Horizon 2020 Grant, Contract No. 675440 (European Union); the Leventis Foundation; the A. P. Sloan Foundation; the Alexander von Humboldt Foundation; the Belgian Federal Science Policy Office; the Fonds pour la Formation à la Recherche dans l’Industrie et dans l’Agriculture (FRIA-Belgium); the Agentschap voor Innovatie door Wetenschap en Technologie (IWT-Belgium); the F.R.S.-FNRS and FWO (Belgium) under the “Excellence of Science - EOS” - be.h project No. 30820817; the Ministry of Education, Youth and Sports (MEYS) of the Czech Republic; the Lendület (“Momentum”) Programme and the János Bolyai Research Scholarship of the Hungarian Academy of Sciences, the New National Excellence Program ÚNKP, the NKFIA Research Grants No. 123842, No. 123959, No. 124845, No. 124850 and No. 125105 (Hungary); the Council of Science and Industrial Research, India; the HOMING PLUS program of the Foundation for Polish Science, cofinanced from European Union, Regional Development Fund, the Mobility Plus program of the Ministry of Science and Higher Education, the National Science Center (Poland), Contracts Harmonia No. 2014/14/M/ST2/00428, Opus No.

2014/13/B/ST2/02543, No. 2014/15/B/ST2/03998, and No. 2015/19/B/ST2/02861, Sonatabis No. 2012/07/E/ST2/01406; the National Priorities Research Program by Qatar National Research Fund; the Programa Estatal de Fomento de la Investigación Científica y Técnica de Excelencia María de Maeztu, Grant No. MDM-2015-0509 and the Programa Severo Ochoa del Principado de Asturias; the Thalis and Aristeia programs cofinanced by EU-ESF and the Greek NSRF; the Rachadapisek Sompot Fund for Postdoctoral Fellowship, Chulalongkorn University and the Chulalongkorn Academic into Its 2nd Century Project Advancement Project (Thailand); the Welch Foundation, Contract No. C-1845; and the Weston Havens Foundation (USA).

References

- [1] Z. Liu and B. Tweedie, “The fate of long-lived superparticles with hadronic decays after LHC Run 1”, *JHEP* **06** (2015) 042, doi:10.1007/JHEP06(2015)042, arXiv:1503.05923.
- [2] G. F. Giudice and A. Romanino, “Split supersymmetry”, *Nucl. Phys. B* **699** (2004) 65, doi:10.1016/j.nuclphysb.2004.08.001, arXiv:hep-ph/0406088. [Erratum: doi:10.1016/j.nuclphysb.2004.11.048].
- [3] J. L. Hewett, B. Lillie, M. Masip, and T. G. Rizzo, “Signatures of long-lived gluinos in split supersymmetry”, *JHEP* **09** (2004) 070, doi:10.1088/1126-6708/2004/09/070, arXiv:hep-ph/0408248.
- [4] N. Arkani-Hamed, S. Dimopoulos, G. F. Giudice, and A. Romanino, “Aspects of split supersymmetry”, *Nucl. Phys. B* **709** (2005) 3, doi:10.1016/j.nuclphysb.2004.12.026, arXiv:hep-ph/0409232.
- [5] P. Gambino, G. F. Giudice, and P. Slavich, “Gluino decays in split supersymmetry”, *Nucl. Phys. B* **726** (2005) 35, doi:10.1016/j.nuclphysb.2005.08.011, arXiv:hep-ph/0506214.
- [6] A. Arvanitaki, N. Craig, S. Dimopoulos, and G. Villadoro, “Mini-split”, *JHEP* **02** (2013) 126, doi:10.1007/JHEP02(2013)126, arXiv:1210.0555.
- [7] N. Arkani-Hamed et al., “Simply unnatural supersymmetry”, (2012). arXiv:1212.6971.
- [8] P. Fayet, “Supergauge invariant extension of the Higgs mechanism and a model for the electron and its neutrino”, *Nucl. Phys. B* **90** (1975) 104, doi:10.1016/0550-3213(75)90636-7.
- [9] G. R. Farrar and P. Fayet, “Phenomenology of the production, decay, and detection of new hadronic states associated with supersymmetry”, *Phys. Lett. B* **76** (1978) 575, doi:10.1016/0370-2693(78)90858-4.
- [10] S. Weinberg, “Supersymmetry at ordinary energies. 1. masses and conservation laws”, *Phys. Rev. D* **26** (1982) 287, doi:10.1103/PhysRevD.26.287.
- [11] R. Barbier et al., “ R -parity violating supersymmetry”, *Phys. Rept.* **420** (2005) 1, doi:10.1016/j.physrep.2005.08.006, arXiv:hep-ph/0406039.
- [12] G. F. Giudice and R. Rattazzi, “Theories with gauge mediated supersymmetry breaking”, *Phys. Rept.* **322** (1999) 419, doi:10.1016/S0370-1573(99)00042-3, arXiv:hep-ph/9801271.

- [13] P. Meade, N. Seiberg, and D. Shih, “General gauge mediation”, *Prog. Theor. Phys. Suppl.* **177** (2009) 143, doi:[10.1143/PTPS.177.143](https://doi.org/10.1143/PTPS.177.143), arXiv:[0801.3278](https://arxiv.org/abs/0801.3278).
- [14] M. Buican, P. Meade, N. Seiberg, and D. Shih, “Exploring general gauge mediation”, *JHEP* **03** (2009) 016, doi:[10.1088/1126-6708/2009/03/016](https://doi.org/10.1088/1126-6708/2009/03/016), arXiv:[0812.3668](https://arxiv.org/abs/0812.3668).
- [15] J. Fan, M. Reece, and J. T. Ruderman, “Stealth supersymmetry”, *JHEP* **11** (2011) 012, doi:[10.1007/JHEP11\(2011\)012](https://doi.org/10.1007/JHEP11(2011)012), arXiv:[1105.5135](https://arxiv.org/abs/1105.5135).
- [16] J. Fan, M. Reece, and J. T. Ruderman, “A stealth supersymmetry sampler”, *JHEP* **07** (2012) 196, doi:[10.1007/JHEP07\(2012\)196](https://doi.org/10.1007/JHEP07(2012)196), arXiv:[1201.4875](https://arxiv.org/abs/1201.4875).
- [17] M. J. Strassler and K. M. Zurek, “Echoes of a hidden valley at hadron colliders”, *Phys. Lett. B* **651** (2007) 374, doi:[10.1016/j.physletb.2007.06.055](https://doi.org/10.1016/j.physletb.2007.06.055), arXiv:[hep-ph/0604261](https://arxiv.org/abs/hep-ph/0604261).
- [18] M. J. Strassler and K. M. Zurek, “Discovering the Higgs through highly-displaced vertices”, *Phys. Lett. B* **661** (2008) 263, doi:[10.1016/j.physletb.2008.02.008](https://doi.org/10.1016/j.physletb.2008.02.008), arXiv:[hep-ph/0605193](https://arxiv.org/abs/hep-ph/0605193).
- [19] T. Han, Z. Si, K. M. Zurek, and M. J. Strassler, “Phenomenology of hidden valleys at hadron colliders”, *JHEP* **07** (2008) 008, doi:[10.1088/1126-6708/2008/07/008](https://doi.org/10.1088/1126-6708/2008/07/008), arXiv:[0712.2041](https://arxiv.org/abs/0712.2041).
- [20] Y. Cui, L. Randall, and B. Shuve, “A WIMPY baryogenesis miracle”, *JHEP* **04** (2012) 075, doi:[10.1007/JHEP04\(2012\)075](https://doi.org/10.1007/JHEP04(2012)075), arXiv:[1112.2704](https://arxiv.org/abs/1112.2704).
- [21] Y. Cui and R. Sundrum, “Baryogenesis for weakly interacting massive particles”, *Phys. Rev. D* **87** (2013) 116013, doi:[10.1103/PhysRevD.87.116013](https://doi.org/10.1103/PhysRevD.87.116013), arXiv:[1212.2973](https://arxiv.org/abs/1212.2973).
- [22] Y. Cui and B. Shuve, “Probing baryogenesis with displaced vertices at the LHC”, *JHEP* **02** (2015) 049, doi:[10.1007/JHEP02\(2015\)049](https://doi.org/10.1007/JHEP02(2015)049), arXiv:[1409.6729](https://arxiv.org/abs/1409.6729).
- [23] Z. Chacko, H.-S. Goh, and R. Harnik, “Natural electroweak breaking from a mirror symmetry”, *Phys. Rev. Lett.* **96** (2006) 231802, doi:[10.1103/PhysRevLett.96.231802](https://doi.org/10.1103/PhysRevLett.96.231802), arXiv:[hep-ph/0506256](https://arxiv.org/abs/hep-ph/0506256).
- [24] D. Curtin and C. B. Verhaaren, “Discovering uncolored naturalness in exotic Higgs decays”, *JHEP* **12** (2015) 072, doi:[10.1007/JHEP12\(2015\)072](https://doi.org/10.1007/JHEP12(2015)072), arXiv:[1506.06141](https://arxiv.org/abs/1506.06141).
- [25] H.-C. Cheng, S. Jung, E. Salvioni, and Y. Tsai, “Exotic quarks in twin Higgs models”, *JHEP* **03** (2016) 074, doi:[10.1007/JHEP03\(2016\)074](https://doi.org/10.1007/JHEP03(2016)074), arXiv:[1512.02647](https://arxiv.org/abs/1512.02647).
- [26] CMS Collaboration, “The CMS experiment at the CERN LHC”, *JINST* **3** (2008) S08004, doi:[10.1088/1748-0221/3/08/S08004](https://doi.org/10.1088/1748-0221/3/08/S08004).
- [27] ATLAS Collaboration, “Search for long-lived, weakly interacting particles that decay to displaced hadronic jets in proton-proton collisions at $\sqrt{s} = 8$ TeV with the ATLAS detector”, *Phys. Rev. D* **92** (2015) 012010, doi:[10.1103/PhysRevD.92.012010](https://doi.org/10.1103/PhysRevD.92.012010), arXiv:[1504.03634](https://arxiv.org/abs/1504.03634).
- [28] ATLAS Collaboration, “Search for massive, long-lived particles using multitrack displaced vertices or displaced lepton pairs in pp collisions at $\sqrt{s} = 8$ TeV with the ATLAS detector”, *Phys. Rev. D* **92** (2015) 072004, doi:[10.1103/PhysRevD.92.072004](https://doi.org/10.1103/PhysRevD.92.072004), arXiv:[1504.05162](https://arxiv.org/abs/1504.05162).

- [29] CMS Collaboration, “Search for long-lived neutral particles decaying to quark-antiquark pairs in proton-proton collisions at $\sqrt{s} = 8$ TeV”, *Phys. Rev. D* **91** (2015) 012007, doi:[10.1103/PhysRevD.91.012007](https://doi.org/10.1103/PhysRevD.91.012007), arXiv:[1411.6530](https://arxiv.org/abs/1411.6530).
- [30] CMS Collaboration, “Search for displaced supersymmetry in events with an electron and a muon with large impact parameters”, *Phys. Rev. Lett.* **114** (2015) 061801, doi:[10.1103/PhysRevLett.114.061801](https://doi.org/10.1103/PhysRevLett.114.061801), arXiv:[1409.4789](https://arxiv.org/abs/1409.4789).
- [31] CMS Collaboration, “Search for R -parity violating supersymmetry with displaced vertices in proton-proton collisions at $\sqrt{s} = 8$ TeV”, *Phys. Rev. D* **95** (2017) 012009, doi:[10.1103/PhysRevD.95.012009](https://doi.org/10.1103/PhysRevD.95.012009), arXiv:[1610.05133](https://arxiv.org/abs/1610.05133).
- [32] LHCb Collaboration, “Search for long-lived particles decaying to jet pairs”, *Eur. Phys. J. C* **75** (2015) 152, doi:[10.1140/epjc/s10052-015-3344-6](https://doi.org/10.1140/epjc/s10052-015-3344-6), arXiv:[1412.3021](https://arxiv.org/abs/1412.3021).
- [33] LHCb Collaboration, “Search for Higgs-like bosons decaying into long-lived exotic particles”, *Eur. Phys. J. C* **76** (2016) 664, doi:[10.1140/epjc/s10052-016-4489-7](https://doi.org/10.1140/epjc/s10052-016-4489-7), arXiv:[1609.03124](https://arxiv.org/abs/1609.03124).
- [34] ATLAS Collaboration, “Search for long-lived, massive particles in events with displaced vertices and missing transverse momentum in $\sqrt{s} = 13$ TeV pp collisions with the ATLAS detector”, *Phys. Rev. D* **97** (2018) 052012, doi:[10.1103/PhysRevD.97.052012](https://doi.org/10.1103/PhysRevD.97.052012), arXiv:[1710.04901](https://arxiv.org/abs/1710.04901).
- [35] CMS Collaboration, “Search for new long-lived particles at $\sqrt{s} = 13$ TeV”, *Phys. Lett. B* **780** (2018) 432, doi:[10.1016/j.physletb.2018.03.019](https://doi.org/10.1016/j.physletb.2018.03.019), arXiv:[1711.09120](https://arxiv.org/abs/1711.09120).
- [36] CMS Collaboration, “Search for long-lived particles with displaced vertices in multijet events in proton-proton collisions at $\sqrt{s} = 13$ TeV”, *Phys. Rev. D* **98** (2018) 092011, doi:[10.1103/PhysRevD.98.092011](https://doi.org/10.1103/PhysRevD.98.092011), arXiv:[1808.03078](https://arxiv.org/abs/1808.03078).
- [37] CMS Collaboration, “Description and performance of track and primary-vertex reconstruction with the CMS tracker”, *JINST* **9** (2014) P10009, doi:[10.1088/1748-0221/9/10/P10009](https://doi.org/10.1088/1748-0221/9/10/P10009), arXiv:[1405.6569](https://arxiv.org/abs/1405.6569).
- [38] CMS Collaboration, “The CMS trigger system”, *JINST* **12** (2017) P01020, doi:[10.1088/1748-0221/12/01/P01020](https://doi.org/10.1088/1748-0221/12/01/P01020), arXiv:[1609.02366](https://arxiv.org/abs/1609.02366).
- [39] M. Cacciari, G. P. Salam, and G. Soyez, “The anti- k_T jet clustering algorithm”, *JHEP* **04** (2008) 063, doi:[10.1088/1126-6708/2008/04/063](https://doi.org/10.1088/1126-6708/2008/04/063), arXiv:[0802.1189](https://arxiv.org/abs/0802.1189).
- [40] M. Cacciari, G. P. Salam, and G. Soyez, “FastJet user manual”, *Eur. Phys. J. C* **72** (2012) 1896, doi:[10.1140/epjc/s10052-012-1896-2](https://doi.org/10.1140/epjc/s10052-012-1896-2), arXiv:[1111.6097](https://arxiv.org/abs/1111.6097).
- [41] CMS Collaboration, “Jet energy scale and resolution in the CMS experiment in pp collisions at 8 TeV”, *JINST* **12** (2017) P02014, doi:[10.1088/1748-0221/12/02/P02014](https://doi.org/10.1088/1748-0221/12/02/P02014), arXiv:[1607.03663](https://arxiv.org/abs/1607.03663).
- [42] CMS Collaboration, “Technical proposal for the Phase-II upgrade of the CMS detector”, CMS Technical proposal CERN-LHCC-2015-010, CMS-TDR-15-02, CERN, 2015.
- [43] J. Alwall et al., “The automated computation of tree-level and next-to-leading order differential cross sections, and their matching to parton shower simulations”, *JHEP* **07** (2014) 079, doi:[10.1007/JHEP07\(2014\)079](https://doi.org/10.1007/JHEP07(2014)079), arXiv:[1405.0301](https://arxiv.org/abs/1405.0301).

- [44] T. Sjöstrand et al., “An introduction to PYTHIA 8.2”, *Comput. Phys. Commun.* **191** (2015) 159, doi:10.1016/j.cpc.2015.01.024, arXiv:1410.3012.
- [45] J. Alwall et al., “Comparative study of various algorithms for the merging of parton showers and matrix elements in hadronic collisions”, *Eur. Phys. J. C* **53** (2008) 473, doi:10.1140/epjc/s10052-007-0490-5, arXiv:0706.2569.
- [46] CMS Collaboration, “Event generator tunes obtained from underlying event and multiparton scattering measurements”, *Eur. Phys. J. C* **76** (2016) 155, doi:10.1140/epjc/s10052-016-3988-x, arXiv:1512.00815.
- [47] NNPDF Collaboration, “Parton distributions for the LHC Run II”, *JHEP* **04** (2015) 040, doi:10.1007/JHEP04(2015)040, arXiv:1410.8849.
- [48] C. Csaki, Y. Grossman, and B. Heidenreich, “Minimal flavor violation supersymmetry: a natural theory for R -parity violation”, *Phys. Rev. D* **85** (2012) 095009, doi:10.1103/PhysRevD.85.095009, arXiv:1111.1239.
- [49] P. W. Graham, D. E. Kaplan, S. Rajendran, and P. Saraswat, “Displaced supersymmetry”, *JHEP* **07** (2012) 149, doi:10.1007/JHEP07(2012)149, arXiv:1204.6038.
- [50] C. Csaki, E. Kuflik, and T. Volansky, “Dynamical R -parity violation”, *Phys. Rev. Lett.* **112** (2014) 131801, doi:10.1103/PhysRevLett.112.131801, arXiv:1309.5957.
- [51] C. Csaki, E. Kuflik, O. Slone, and T. Volansky, “Models of dynamical R -parity violation”, *JHEP* **06** (2015) 045, doi:10.1007/JHEP06(2015)045, arXiv:1502.03096.
- [52] C. Csaki et al., “Phenomenology of a long-lived LSP with R -parity violation”, *JHEP* **08** (2015) 016, doi:10.1007/JHEP08(2015)016, arXiv:1505.00784.
- [53] NNPDF Collaboration, “Parton distributions with QED corrections”, *Nucl. Phys. B* **877** (2013) 290, doi:10.1016/j.nuclphysb.2013.10.010, arXiv:1308.0598.
- [54] G. R. Farrar and P. Fayet, “Bounds on R -hadron production from calorimetry experiments”, *Phys. Lett. B* **79** (1978) 442, doi:10.1016/0370-2693(78)90402-1.
- [55] M. Fairbairn et al., “Stable massive particles at colliders”, *Phys. Rept.* **438** (2007) 1, doi:10.1016/j.physrep.2006.10.002, arXiv:hep-ph/0611040.
- [56] GEANT4 Collaboration, “GEANT4—a simulation toolkit”, *Nucl. Instrum. Meth. A* **506** (2003) 250, doi:10.1016/S0168-9002(03)01368-8.
- [57] R. Frühwirth, W. Waltenberger, and P. Vanlaer, “Adaptive vertex fitting”, *J. Phys. G* **34** (2007) N343, doi:10.1088/0954-3899/34/12/N01.
- [58] S. C. Johnson, “Hierarchical clustering schemes”, *Psychometrika* **32** (1967) 241, doi:10.1007/BF02289588.
- [59] CMS Collaboration, “CMS luminosity measurements for the 2016 data taking period”, CMS Physics Analysis Summary CMS-PAS-LUM-17-001, 2017.
- [60] S. Dulat et al., “New parton distribution functions from a global analysis of quantum chromodynamics”, *Phys. Rev. D* **93** (2016) 033006, doi:10.1103/PhysRevD.93.033006, arXiv:1506.07443.

- [61] L. A. Harland-Lang, A. D. Martin, P. Motylinski, and R. S. Thorne, “Parton distributions in the LHC era: MMHT 2014 PDFs”, *Eur. Phys. J. C* **75** (2015) 204, doi:10.1140/epjc/s10052-015-3397-6, arXiv:1412.3989.
- [62] J. Butterworth et al., “PDF4LHC recommendations for LHC Run II”, *J. Phys. G* **43** (2016) 023001, doi:10.1088/0954-3899/43/2/023001, arXiv:1510.03865.
- [63] A. Buckley et al., “LHAPDF6: parton density access in the LHC precision era”, *Eur. Phys. J. C* **75** (2015) 132, doi:10.1140/epjc/s10052-015-3318-8, arXiv:1412.7420.
- [64] T. Junk, “Confidence level computation for combining searches with small statistics”, *Nucl. Instrum. Meth. A* **434** (1999) 435, doi:10.1016/S0168-9002(99)00498-2, arXiv:hep-ex/9902006.
- [65] A. L. Read, “Presentation of search results: The CL_s technique”, *J. Phys. G* **28** (2002) 2693, doi:10.1088/0954-3899/28/10/313.
- [66] G. Cowan, K. Cranmer, E. Gross, and O. Vitells, “Asymptotic formulae for likelihood-based tests of new physics”, *Eur. Phys. J. C* **71** (2011) 1554, doi:10.1140/epjc/s10052-011-1554-0, arXiv:1007.1727. [Erratum: doi:10.1140/epjc/s10052-013-2501-z].
- [67] The ATLAS Collaboration, The CMS Collaboration, The LHC Higgs Combination Group, “Procedure for the LHC Higgs boson search combination in Summer 2011”, Technical Report CMS-NOTE-2011-005, ATL-PHYS-PUB-2011-11, 2011.
- [68] W. Beenakker, R. Hopker, M. Spira, and P. M. Zerwas, “Squark and gluino production at hadron colliders”, *Nucl. Phys. B* **492** (1997) 51, doi:10.1016/S0550-3213(97)80027-2, arXiv:hep-ph/9610490.
- [69] A. Kulesza and L. Motyka, “Threshold resummation for squark-antisquark and gluino-pair production at the LHC”, *Phys. Rev. Lett.* **102** (2009) 111802, doi:10.1103/PhysRevLett.102.111802, arXiv:0807.2405.
- [70] A. Kulesza and L. Motyka, “Soft gluon resummation for the production of gluino-gluino and squark-antisquark pairs at the LHC”, *Phys. Rev. D* **80** (2009) 095004, doi:10.1103/PhysRevD.80.095004, arXiv:0905.4749.
- [71] W. Beenakker et al., “Squark and gluino hadroproduction”, *Int. J. Mod. Phys. A* **26** (2011) 2637, doi:10.1142/S0217751X11053560, arXiv:1105.1110.
- [72] C. Borschensky et al., “Squark and gluino production cross sections in pp collisions at $\sqrt{s} = 13, 14, 33$ and 100 TeV”, *Eur. Phys. J. C* **74** (2014) 3174, doi:10.1140/epjc/s10052-014-3174-y, arXiv:1407.5066.

A Supplemental information

Tables 6–10 summarize the signal efficiencies for representative signal points in jet-jet, $\tilde{g} \rightarrow g\tilde{G}$, $\tilde{g} \rightarrow tbs$, $\tilde{t} \rightarrow b\ell$, and $\tilde{t} \rightarrow d\bar{d}$ models. Figure 8 shows the comparison with the search for displaced vertices in multijet events at $\sqrt{s} = 13$ TeV with the CMS detector [36], for $\tilde{g} \rightarrow tbs$ and $\tilde{t} \rightarrow d\bar{d}$ models.

Table 6: Signal efficiencies (in %) for the jet-jet model at different proper decay lengths $c\tau_0$ and different masses m_X . Selection requirements are cumulative from the first row to the last. Uncertainties are statistical only.

Efficiency (%)	m_X (GeV)	$c\tau_0$			
		1 mm	10 mm	100 mm	1000 mm
Trigger		20.32 ± 0.45	82.96 ± 0.91	64.58 ± 0.80	12.94 ± 0.36
Preselection	1000	17.99 ± 0.42	80.54 ± 0.90	61.40 ± 0.78	11.29 ± 0.34
Final selection		9.69 ± 0.31	57.23 ± 0.76	44.86 ± 0.67	7.79 ± 0.28
Trigger		18.86 ± 0.43	69.00 ± 0.83	42.44 ± 0.65	6.27 ± 0.25
Preselection	300	14.22 ± 0.37	60.94 ± 0.78	36.53 ± 0.60	4.83 ± 0.22
Final selection		6.98 ± 0.26	39.51 ± 0.63	22.0 ± 0.47	2.82 ± 0.17
Trigger		3.10 ± 0.10	10.3 ± 0.18	4.91 ± 0.13	0.50 ± 0.04
Preselection	100	2.13 ± 0.08	7.91 ± 0.16	3.48 ± 0.11	0.34 ± 0.03
Final selection		0.92 ± 0.06	4.41 ± 0.12	1.64 ± 0.07	0.17 ± 0.02

Table 7: Signal efficiencies (in %) for pair produced long-lived gluinos decaying to a gluon and a gravitino at different proper decay lengths $c\tau_0$ and different gluino masses $m_{\tilde{g}}$. Selection requirements are cumulative from the first row to the last. Uncertainties are statistical only.

Efficiency (%)	$m_{\tilde{g}}$ (GeV)	$c\tau_0$			
		1 mm	10 mm	100 mm	1000 mm
Trigger		6.58 ± 0.12	62.49 ± 0.35	75.45 ± 0.39	27.55 ± 0.25
Preselection	2400	4.80 ± 0.10	57.62 ± 0.34	68.36 ± 0.37	22.58 ± 0.21
Final selection		2.02 ± 0.06	31.73 ± 0.25	43.45 ± 0.29	14.18 ± 0.17
Trigger		7.43 ± 0.12	61.48 ± 0.35	70.12 ± 0.37	22.31 ± 0.21
Preselection	1800	5.56 ± 0.11	56.05 ± 0.33	62.05 ± 0.35	18.05 ± 0.19
Final selection		2.19 ± 0.07	29.91 ± 0.24	37.73 ± 0.27	10.88 ± 0.15
Trigger		7.42 ± 0.13	55.92 ± 0.34	57.58 ± 0.34	13.71 ± 0.16
Preselection	1000	5.47 ± 0.11	48.55 ± 0.31	47.13 ± 0.31	10.52 ± 0.15
Final selection		1.96 ± 0.06	23.48 ± 0.22	25.78 ± 0.23	5.52 ± 0.11

Table 8: Signal efficiencies (in %) for pair produced long-lived gluinos decaying to top, bottom and strange antiquarks at different proper decay lengths $c\tau_0$ and different gluino masses $m_{\tilde{g}}$. Selection requirements are cumulative from the first row to the last. Uncertainties are statistical only.

Efficiency (%)	$m_{\tilde{g}}$ (GeV)	$c\tau_0$			
		1 mm	10 mm	100 mm	1000 mm
Trigger		12.53 ± 0.41	80.30 ± 4.90	85.00 ± 1.10	33.83 ± 0.41
Preselection	2400	10.48 ± 0.37	79.70 ± 4.88	84.57 ± 1.10	32.01 ± 0.40
Final selection		4.42 ± 0.24	51.04 ± 3.90	60.35 ± 0.93	21.55 ± 0.33
Trigger		14.95 ± 0.28	78.94 ± 0.64	82.93 ± 0.65	28.81 ± 0.38
Preselection	1800	10.48 ± 0.37	79.70 ± 4.88	84.57 ± 1.10	32.01 ± 0.40
Final selection		4.42 ± 0.24	51.04 ± 3.90	60.35 ± 0.93	21.55 ± 0.33
Trigger		18.30 ± 0.30	78.32 ± 0.63	77.75 ± 0.63	23.39 ± 0.34
Preselection	1200	15.21 ± 0.28	76.92 ± 0.62	76.94 ± 0.63	21.45 ± 0.33
Final selection		5.21 ± 0.16	43.01 ± 0.47	48.40 ± 0.50	12.03 ± 0.24

Table 9: Signal efficiencies (in %) for pair produced long-lived top squarks decaying to a bottom quark and a lepton at different proper decay lengths $c\tau_0$ and different top squark masses $m_{\tilde{t}}$. Selection requirements are cumulative from the first row to the last. Uncertainties are statistical only.

Efficiency (%)	$m_{\tilde{t}}$ (GeV)	$c\tau_0$			
		1 mm	10 mm	100 mm	1000 mm
Trigger		6.44 ± 0.19	48.12 ± 0.52	46.33 ± 0.53	12.02 ± 0.26
Preselection	1500	3.79 ± 0.14	37.11 ± 0.45	32.39 ± 0.45	6.24 ± 0.19
Final selection		1.57 ± 0.09	20.53 ± 0.34	17.47 ± 0.33	3.02 ± 0.13
Trigger		6.68 ± 0.09	46.25 ± 0.23	42.98 ± 0.21	8.71 ± 0.10
Preselection	1200	4.34 ± 0.07	38.28 ± 0.21	33.62 ± 0.19	5.83 ± 0.08
Final selection		1.55 ± 0.04	18.41 ± 0.14	16.54 ± 0.14	2.63 ± 0.05
Trigger		6.99 ± 0.08	41.12 ± 0.21	32.65 ± 0.19	5.28 ± 0.08
Preselection	600	3.53 ± 0.06	29.69 ± 0.18	22.34 ± 0.16	3.06 ± 0.06
Final selection		0.88 ± 0.03	11.63 ± 0.11	8.71 ± 0.10	1.10 ± 0.03

Table 10: Signal efficiencies (in %) for pair produced long-lived top squarks decaying to two down antiquarks at different proper decay lengths $c\tau_0$ and different top squark masses $m_{\tilde{t}}$. Selection requirements are cumulative from the first row to the last. Uncertainties are statistical only.

Efficiency (%)	$m_{\tilde{t}}$ (GeV)	$c\tau_0$			
		1 mm	10 mm	100 mm	1000 mm
Trigger		12.05 ± 0.25	74.66 ± 0.62	77.19 ± 0.98	24.03 ± 0.54
Preselection	1600	10.27 ± 0.23	72.70 ± 0.61	75.01 ± 0.97	21.43 ± 0.51
Final selection		5.36 ± 0.16	48.75 ± 0.50	53.59 ± 0.81	14.65 ± 0.42
Trigger		12.31 ± 0.25	73.74 ± 0.61	73.92 ± 0.61	20.26 ± 0.48
Preselection	1200	10.46 ± 0.23	71.55 ± 0.60	71.36 ± 0.60	18.04 ± 0.45
Final selection		5.13 ± 0.16	48.04 ± 0.49	49.44 ± 0.50	12.27 ± 0.37
Trigger		12.02 ± 0.37	71.75 ± 0.89	67.03 ± 0.92	16.27 ± 0.29
Preselection	600	9.97 ± 0.33	69.08 ± 0.88	63.60 ± 0.89	14.38 ± 0.26
Final selection		4.90 ± 0.23	45.68 ± 0.71	42.61 ± 0.72	9.08 ± 0.21

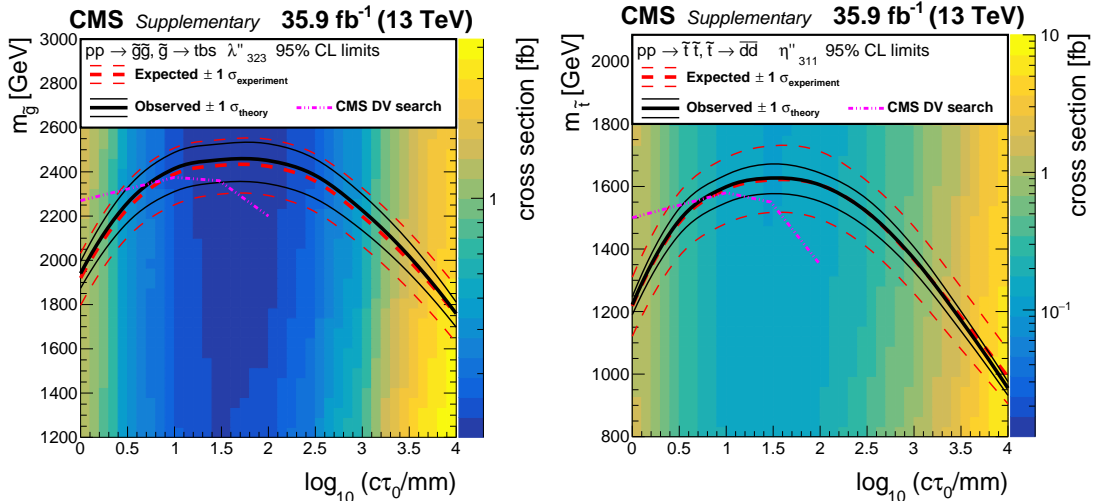


Figure 8: Comparison with search for displaced vertices in multijet events at $\sqrt{s} = 13$ TeV with the CMS detector [36] (referred to as the CMS DV search) for $\tilde{g} \rightarrow \text{tbs}$ (left) and $\tilde{t} \rightarrow \bar{d}\bar{d}$ (right) models. The CMS DV search looks for a pair of displaced vertices within the beam pipe. The observed limits obtained by the CMS DV search (purple curves) are overlaid with the limits obtained by the search presented in this paper in the mass-lifetime plane, and are good complements for proper decay length $c\tau_0 < 10$ mm in these two signal models.

B The CMS Collaboration

Yerevan Physics Institute, Yerevan, Armenia

A.M. Sirunyan, A. Tumasyan

Institut für Hochenergiephysik, Wien, Austria

W. Adam, F. Ambrogi, E. Asilar, T. Bergauer, J. Brandstetter, M. Dragicevic, J. Erö, A. Escalante Del Valle, M. Flechl, R. Frühwirth¹, V.M. Ghete, J. Hrubec, M. Jeitler¹, N. Krammer, I. Krätschmer, D. Liko, T. Madlener, I. Mikulec, N. Rad, H. Rohringer, J. Schieck¹, R. Schöfbeck, M. Spanring, D. Spitzbart, W. Waltenberger, J. Wittmann, C.-E. Wulz¹, M. Zarucki

Institute for Nuclear Problems, Minsk, Belarus

V. Chekhovsky, V. Mossolov, J. Suarez Gonzalez

Universiteit Antwerpen, Antwerpen, Belgium

E.A. De Wolf, D. Di Croce, X. Janssen, J. Lauwers, A. Lelek, M. Pieters, H. Van Haevermaet, P. Van Mechelen, N. Van Remortel

Vrije Universiteit Brussel, Brussel, Belgium

S. Abu Zeid, F. Blekman, J. D'Hondt, J. De Clercq, K. Deroover, G. Flouris, D. Lontkovskyi, S. Lowette, I. Marchesini, S. Moortgat, L. Moreels, Q. Python, K. Skovpen, S. Tavernier, W. Van Doninck, P. Van Mulders, I. Van Parijs

Université Libre de Bruxelles, Bruxelles, Belgium

D. Beghin, B. Bilin, H. Brun, B. Clerbaux, G. De Lentdecker, H. Delannoy, B. Dorney, G. Fasanella, L. Favart, A. Grebenyuk, A.K. Kalsi, T. Lenzi, J. Luetic, N. Postiau, E. Starling, L. Thomas, C. Vander Velde, P. Vanlaer, D. Vannerom, Q. Wang

Ghent University, Ghent, Belgium

T. Cornelis, D. Dobur, A. Fagot, M. Gul, I. Khvastunov², D. Poyraz, C. Roskas, D. Trocino, M. Tytgat, W. Verbeke, B. Vermassen, M. Vit, N. Zaganidis

Université Catholique de Louvain, Louvain-la-Neuve, Belgium

H. Bakhshiansohi, O. Bondi, S. Brochet, G. Bruno, C. Caputo, P. David, C. Delaere, M. Delcourt, A. Giannanco, G. Krintiras, V. Lemaitre, A. Magitteri, K. Piotrzkowski, A. Saggio, M. Vidal Marono, P. Vischia, S. Wertz, J. Zobec

Centro Brasileiro de Pesquisas Fisicas, Rio de Janeiro, Brazil

F.L. Alves, G.A. Alves, G. Correia Silva, C. Hensel, A. Moraes, M.E. Pol, P. Rebello Teles

Universidade do Estado do Rio de Janeiro, Rio de Janeiro, Brazil

E. Belchior Batista Das Chagas, W. Carvalho, J. Chinellato³, E. Coelho, E.M. Da Costa, G.G. Da Silveira⁴, D. De Jesus Damiao, C. De Oliveira Martins, S. Fonseca De Souza, H. Malbouisson, D. Matos Figueiredo, M. Melo De Almeida, C. Mora Herrera, L. Mundim, H. Nogima, W.L. Prado Da Silva, L.J. Sanchez Rosas, A. Santoro, A. Sznajder, M. Thiel, E.J. Tonelli Manganote³, F. Torres Da Silva De Araujo, A. Vilela Pereira

Universidade Estadual Paulista ^a, Universidade Federal do ABC ^b, São Paulo, Brazil

S. Ahuja^a, C.A. Bernardes^a, L. Calligaris^a, T.R. Fernandez Perez Tomei^a, E.M. Gregores^b, P.G. Mercadante^b, S.F. Novaes^a, SandraS. Padula^a

Institute for Nuclear Research and Nuclear Energy, Bulgarian Academy of Sciences, Sofia, Bulgaria

A. Aleksandrov, R. Hadjiiska, P. Iaydjiev, A. Marinov, M. Misheva, M. Rodozov, M. Shopova, G. Sultanov

University of Sofia, Sofia, Bulgaria

A. Dimitrov, L. Litov, B. Pavlov, P. Petkov

Beihang University, Beijing, China

W. Fang⁵, X. Gao⁵, L. Yuan

Institute of High Energy Physics, Beijing, China

M. Ahmad, J.G. Bian, G.M. Chen, H.S. Chen, M. Chen, Y. Chen, C.H. Jiang, D. Leggat, H. Liao, Z. Liu, S.M. Shaheen⁶, A. Spiezja, J. Tao, E. Yazgan, H. Zhang, S. Zhang⁶, J. Zhao

State Key Laboratory of Nuclear Physics and Technology, Peking University, Beijing, China

Y. Ban, G. Chen, A. Levin, J. Li, L. Li, Q. Li, Y. Mao, S.J. Qian, D. Wang

Tsinghua University, Beijing, China

Y. Wang

Universidad de Los Andes, Bogota, Colombia

C. Avila, A. Cabrera, C.A. Carrillo Montoya, L.F. Chaparro Sierra, C. Florez, C.F. González Hernández, M.A. Segura Delgado

University of Split, Faculty of Electrical Engineering, Mechanical Engineering and Naval Architecture, Split, Croatia

B. Courbon, N. Godinovic, D. Lelas, I. Puljak, T. Sculac

University of Split, Faculty of Science, Split, Croatia

Z. Antunovic, M. Kovac

Institute Rudjer Boskovic, Zagreb, Croatia

V. Brigljevic, D. Ferencek, K. Kadija, B. Mesic, M. Roguljic, A. Starodumov⁷, T. Susa

University of Cyprus, Nicosia, Cyprus

M.W. Ather, A. Attikis, M. Kolosova, G. Mavromanolakis, J. Mousa, C. Nicolaou, F. Ptochos, P.A. Razis, H. Rykaczewski

Charles University, Prague, Czech Republic

M. Finger⁸, M. Finger Jr.⁸

Escuela Politecnica Nacional, Quito, Ecuador

E. Ayala

Universidad San Francisco de Quito, Quito, Ecuador

E. Carrera Jarrin

Academy of Scientific Research and Technology of the Arab Republic of Egypt, Egyptian Network of High Energy Physics, Cairo, Egypt

S. Elgammal⁹, A. Mahrous¹⁰, Y. Mohammed¹¹

National Institute of Chemical Physics and Biophysics, Tallinn, Estonia

S. Bhowmik, A. Carvalho Antunes De Oliveira, R.K. Dewanjee, K. Ehataht, M. Kadastik, M. Raidal, C. Veelken

Department of Physics, University of Helsinki, Helsinki, Finland

P. Eerola, H. Kirschenmann, J. Pekkanen, M. Voutilainen

Helsinki Institute of Physics, Helsinki, Finland

J. Havukainen, J.K. Heikkilä, T. Järvinen, V. Karimäki, R. Kinnunen, T. Lampén, K. Lassila-Perini, S. Laurila, S. Lehti, T. Lindén, P. Luukka, T. Mäenpää, H. Siikonen, E. Tuominen, J. Tuominiemi

Lappeenranta University of Technology, Lappeenranta, Finland

T. Tuuva

IRFU, CEA, Université Paris-Saclay, Gif-sur-Yvette, France

M. Besancon, F. Couderc, M. Dejardin, D. Denegri, J.L. Faure, F. Ferri, S. Ganjour, A. Givernaud, P. Gras, G. Hamel de Monchenault, P. Jarry, C. Leloup, E. Locci, J. Malcles, G. Negro, J. Rander, A. Rosowsky, M.Ö. Sahin, M. Titov

Laboratoire Leprince-Ringuet, Ecole polytechnique, CNRS/IN2P3, Université Paris-Saclay, Palaiseau, France

A. Abdulsalam¹², C. Amendola, I. Antropov, F. Beaudette, P. Busson, C. Charlot, R. Granier de Cassagnac, I. Kucher, A. Lobanov, J. Martin Blanco, C. Martin Perez, M. Nguyen, C. Ochando, G. Ortona, P. Paganini, J. Rembser, R. Salerno, J.B. Sauvan, Y. Sirois, A.G. Stahl Leiton, A. Zabi, A. Zghiche

Université de Strasbourg, CNRS, IPHC UMR 7178, Strasbourg, France

J.-L. Agram¹³, J. Andrea, D. Bloch, J.-M. Brom, E.C. Chabert, V. Cherepanov, C. Collard, E. Conte¹³, J.-C. Fontaine¹³, D. Gelé, U. Goerlach, M. Jansová, A.-C. Le Bihan, N. Tonon, P. Van Hove

Centre de Calcul de l’Institut National de Physique Nucléaire et de Physique des Particules, CNRS/IN2P3, Villeurbanne, France

S. Gadrat

Université de Lyon, Université Claude Bernard Lyon 1, CNRS-IN2P3, Institut de Physique Nucléaire de Lyon, Villeurbanne, France

S. Beauceron, C. Bernet, G. Boudoul, N. Chanon, R. Chierici, D. Contardo, P. Depasse, H. El Mamouni, J. Fay, L. Finco, S. Gascon, M. Gouzevitch, G. Grenier, B. Ille, F. Lagarde, I.B. Laktineh, H. Lattaud, M. Lethuillier, L. Mirabito, S. Perries, A. Popov¹⁴, V. Sordini, G. Touquet, M. Vander Donckt, S. Viret

Georgian Technical University, Tbilisi, Georgia

T. Toriashvili¹⁵

Tbilisi State University, Tbilisi, Georgia

D. Lomidze

RWTH Aachen University, I. Physikalisches Institut, Aachen, Germany

C. Autermann, L. Feld, M.K. Kiesel, K. Klein, M. Lipinski, M. Preuten, M.P. Rauch, C. Schomakers, J. Schulz, M. Teroerde, B. Wittmer

RWTH Aachen University, III. Physikalisches Institut A, Aachen, Germany

A. Albert, D. Duchardt, M. Erdmann, S. Erdweg, T. Esch, R. Fischer, S. Ghosh, A. Güth, T. Hebbeker, C. Heidemann, K. Hoepfner, H. Keller, L. Mastrolorenzo, M. Merschmeyer, A. Meyer, P. Millet, S. Mukherjee, T. Pook, M. Radziej, H. Reithler, M. Rieger, A. Schmidt, D. Teyssier, S. Thüer

RWTH Aachen University, III. Physikalisches Institut B, Aachen, Germany

G. Flügge, O. Hlushchenko, T. Kress, T. Müller, A. Nehrkorn, A. Nowack, C. Pistone, O. Pooth, D. Roy, H. Sert, A. Stahl¹⁶

Deutsches Elektronen-Synchrotron, Hamburg, Germany

M. Aldaya Martin, T. Arndt, C. Asawatangtrakuldee, I. Babounikau, K. Beernaert, O. Behnke, U. Behrens, A. Bermúdez Martínez, D. Bertsche, A.A. Bin Anuar, K. Borras¹⁷, V. Botta, A. Campbell, P. Connor, C. Contreras-Campana, V. Danilov, A. De Wit, M.M. Defranchis, C. Diez Pardos, D. Domínguez Damiani, G. Eckerlin, T. Eichhorn, A. Elwood, E. Eren, E. Gallo¹⁸, A. Geiser, J.M. Grados Luyando, A. Grohsjean, M. Guthoff, M. Haranko, A. Harb, H. Jung, M. Kasemann, J. Keaveney, C. Kleinwort, J. Knolle, D. Krücker, W. Lange, T. Lenz, J. Leonard, K. Lipka, W. Lohmann¹⁹, R. Mankel, I.-A. Melzer-Pellmann, A.B. Meyer, M. Meyer, M. Missiroli, G. Mittag, J. Mnich, V. Myronenko, S.K. Pflitsch, D. Pitzl, A. Raspereza, A. Saibel, M. Savitskyi, P. Saxena, P. Schütze, C. Schwanenberger, R. Shevchenko, A. Singh, H. Tholen, O. Turkot, A. Vagnerini, M. Van De Klundert, G.P. Van Onsem, R. Walsh, Y. Wen, K. Wichmann, C. Wissing, O. Zenaiev

University of Hamburg, Hamburg, Germany

R. Aggleton, S. Bein, L. Benato, A. Benecke, T. Dreyer, A. Ebrahimi, E. Garutti, D. Gonzalez, P. Gunnellini, J. Haller, A. Hinzmann, A. Karavdina, G. Kasieczka, R. Klanner, R. Kogler, N. Kovalchuk, S. Kurz, V. Kutzner, J. Lange, D. Marconi, J. Multhaup, M. Niedziela, C.E.N. Niemeyer, D. Nowatschin, A. Perieanu, A. Reimers, O. Rieger, C. Scharf, P. Schleper, S. Schumann, J. Schwandt, J. Sonneveld, H. Stadie, G. Steinbrück, F.M. Stober, M. Stöver, B. Vormwald, I. Zoi

Karlsruher Institut fuer Technologie, Karlsruhe, Germany

M. Akbiyik, C. Barth, M. Baselga, S. Baur, E. Butz, R. Caspart, T. Chwalek, F. Colombo, W. De Boer, A. Dierlamm, K. El Morabit, N. Faltermann, B. Freund, M. Giffels, M.A. Harrendorf, F. Hartmann¹⁶, S.M. Heindl, U. Husemann, I. Katkov¹⁴, S. Kudella, S. Mitra, M.U. Mozer, Th. Müller, M. Musich, M. Plagge, G. Quast, K. Rabbertz, M. Schröder, I. Shvetsov, H.J. Simonis, R. Ulrich, S. Wayand, M. Weber, T. Weiler, C. Wöhrmann, R. Wolf

Institute of Nuclear and Particle Physics (INPP), NCSR Demokritos, Aghia Paraskevi, Greece

G. Anagnostou, G. Daskalakis, T. Geralis, A. Kyriakis, D. Loukas, G. Paspalaki

National and Kapodistrian University of Athens, Athens, Greece

A. Agapitos, G. Karathanasis, P. Kontaxakis, A. Panagiotou, I. Papavergou, N. Saoulidou, K. Vellidis

National Technical University of Athens, Athens, Greece

K. Kousouris, I. Papakrivopoulos, G. Tsipolitis

University of Ioánnina, Ioánnina, Greece

I. Evangelou, C. Foudas, P. Gianneios, P. Katsoulis, P. Kokkas, S. Mallios, N. Manthos, I. Papadopoulos, E. Paradas, J. Strologas, F.A. Triantis, D. Tsitsonis

MTA-ELTE Lendület CMS Particle and Nuclear Physics Group, Eötvös Loránd University, Budapest, Hungary

M. Bartók²⁰, M. Csanad, N. Filipovic, P. Major, M.I. Nagy, G. Pasztor, O. Surányi, G.I. Veres

Wigner Research Centre for Physics, Budapest, Hungary

G. Bencze, C. Hajdu, D. Horvath²¹, Á. Hunyadi, F. Sikler, T.Á. Vámi, V. Veszpremi, G. Vesztregombi[†]

Institute of Nuclear Research ATOMKI, Debrecen, Hungary

N. Beni, S. Czellar, J. Karancsi²⁰, A. Makovec, J. Molnar, Z. Szillasi

Institute of Physics, University of Debrecen, Debrecen, Hungary
 P. Raics, Z.L. Trocsanyi, B. Ujvari

Indian Institute of Science (IISc), Bangalore, India
 S. Choudhury, J.R. Komaragiri, P.C. Tiwari

National Institute of Science Education and Research, HBNI, Bhubaneswar, India
 S. Bahinipati²³, C. Kar, P. Mal, K. Mandal, A. Nayak²⁴, S. Roy Chowdhury, D.K. Sahoo²³,
 S.K. Swain

Panjab University, Chandigarh, India
 S. Bansal, S.B. Beri, V. Bhatnagar, S. Chauhan, R. Chawla, N. Dhingra, R. Gupta, A. Kaur,
 M. Kaur, S. Kaur, P. Kumari, M. Lohan, M. Meena, A. Mehta, K. Sandeep, S. Sharma, J.B. Singh,
 A.K. Virdi, G. Walia

University of Delhi, Delhi, India
 A. Bhardwaj, B.C. Choudhary, R.B. Garg, M. Gola, S. Keshri, Ashok Kumar, S. Malhotra,
 M. Naimuddin, P. Priyanka, K. Ranjan, Aashaq Shah, R. Sharma

Saha Institute of Nuclear Physics, HBNI, Kolkata, India
 R. Bhardwaj²⁵, M. Bharti²⁵, R. Bhattacharya, S. Bhattacharya, U. Bhawandeep²⁵, D. Bhowmik,
 S. Dey, S. Dutt²⁵, S. Dutta, S. Ghosh, M. Maity²⁶, K. Mondal, S. Nandan, A. Purohit, P.K. Rout,
 A. Roy, G. Saha, S. Sarkar, T. Sarkar²⁶, M. Sharan, B. Singh²⁵, S. Thakur²⁵

Indian Institute of Technology Madras, Madras, India
 P.K. Behera, A. Muhammad

Bhabha Atomic Research Centre, Mumbai, India
 R. Chudasama, D. Dutta, V. Jha, V. Kumar, D.K. Mishra, P.K. Netrakanti, L.M. Pant, P. Shukla,
 P. Suggisetti

Tata Institute of Fundamental Research-A, Mumbai, India
 T. Aziz, M.A. Bhat, S. Dugad, G.B. Mohanty, N. Sur, Ravindra Kumar Verma

Tata Institute of Fundamental Research-B, Mumbai, India
 S. Banerjee, S. Bhattacharya, S. Chatterjee, P. Das, M. Guchait, Sa. Jain, S. Karmakar, S. Kumar,
 G. Majumder, K. Mazumdar, N. Sahoo

Indian Institute of Science Education and Research (IISER), Pune, India
 S. Chauhan, S. Dube, V. Hegde, A. Kapoor, K. Kotheendar, S. Pandey, A. Rane, A. Rastogi,
 S. Sharma

Institute for Research in Fundamental Sciences (IPM), Tehran, Iran
 S. Chenarani²⁷, E. Eskandari Tadavani, S.M. Etesami²⁷, M. Khakzad, M. Mohammadi Na-
 jafabadi, M. Naseri, F. Rezaei Hosseinabadi, B. Safarzadeh²⁸, M. Zeinali

University College Dublin, Dublin, Ireland
 M. Felcini, M. Grunewald

INFN Sezione di Bari ^a, Università di Bari ^b, Politecnico di Bari ^c, Bari, Italy
 M. Abbrescia^{a,b}, C. Calabria^{a,b}, A. Colaleo^a, D. Creanza^{a,c}, L. Cristella^{a,b}, N. De Filippis^{a,c},
 M. De Palma^{a,b}, A. Di Florio^{a,b}, F. Errico^{a,b}, L. Fiore^a, A. Gelmi^{a,b}, G. Iaselli^{a,c}, M. Ince^{a,b},
 S. Lezki^{a,b}, G. Maggi^{a,c}, M. Maggi^a, G. Miniello^{a,b}, S. My^{a,b}, S. Nuzzo^{a,b}, A. Pompili^{a,b},
 G. Pugliese^{a,c}, R. Radogna^a, A. Ranieri^a, G. Selvaggi^{a,b}, A. Sharma^a, L. Silvestris^a, R. Venditti^a,
 P. Verwilligen^a

INFN Sezione di Bologna ^a, Università di Bologna ^b, Bologna, Italy

G. Abbiendi^a, C. Battilana^{a,b}, D. Bonacorsi^{a,b}, L. Borgonovi^{a,b}, S. Braibant-Giacomelli^{a,b}, R. Campanini^{a,b}, P. Capiluppi^{a,b}, A. Castro^{a,b}, F.R. Cavallo^a, S.S. Chhibra^{a,b}, G. Codispoti^{a,b}, M. Cuffiani^{a,b}, G.M. Dallavalle^a, F. Fabbri^a, A. Fanfani^{a,b}, E. Fontanesi, P. Giacomelli^a, C. Grandi^a, L. Guiducci^{a,b}, F. Iemmi^{a,b}, S. Lo Meo^{a,²⁹}, S. Marcellini^a, G. Masetti^a, A. Montanari^a, F.L. Navarria^{a,b}, A. Perrotta^a, F. Primavera^{a,b}, A.M. Rossi^{a,b}, T. Rovelli^{a,b}, G.P. Siroli^{a,b}, N. Tosi^a

INFN Sezione di Catania ^a, Università di Catania ^b, Catania, Italy

S. Albergo^{a,b}, A. Di Mattia^a, R. Potenza^{a,b}, A. Tricomi^{a,b}, C. Tuve^{a,b}

INFN Sezione di Firenze ^a, Università di Firenze ^b, Firenze, Italy

G. Barbagli^a, K. Chatterjee^{a,b}, V. Ciulli^{a,b}, C. Civinini^a, R. D'Alessandro^{a,b}, E. Focardi^{a,b}, G. Latino, P. Lenzi^{a,b}, M. Meschini^a, S. Paoletti^a, L. Russo^{a,³⁰}, G. Sguazzoni^a, D. Strom^a, L. Viliani^a

INFN Laboratori Nazionali di Frascati, Frascati, Italy

L. Benussi, S. Bianco, F. Fabbri, D. Piccolo

INFN Sezione di Genova ^a, Università di Genova ^b, Genova, Italy

F. Ferro^a, R. Mulargia^{a,b}, E. Robutti^a, S. Tosi^{a,b}

INFN Sezione di Milano-Bicocca ^a, Università di Milano-Bicocca ^b, Milano, Italy

A. Benaglia^a, A. Beschi^b, F. Brivio^{a,b}, V. Ciriolo^{a,b,¹⁶}, S. Di Guida^{a,b,¹⁶}, M.E. Dinardo^{a,b}, S. Fiorendi^{a,b}, S. Gennai^a, A. Ghezzi^{a,b}, P. Govoni^{a,b}, M. Malberti^{a,b}, S. Malvezzi^a, D. Menasce^a, F. Monti, L. Moroni^a, M. Paganoni^{a,b}, D. Pedrini^a, S. Ragazzi^{a,b}, T. Tabarelli de Fatis^{a,b}, D. Zuolo^{a,b}

INFN Sezione di Napoli ^a, Università di Napoli 'Federico II' ^b, Napoli, Italy, Università della Basilicata ^c, Potenza, Italy, Università G. Marconi ^d, Roma, Italy

S. Buontempo^a, N. Cavallo^{a,c}, A. De Iorio^{a,b}, A. Di Crescenzo^{a,b}, F. Fabozzi^{a,c}, F. Fienga^a, G. Galati^a, A.O.M. Iorio^{a,b}, L. Lista^a, S. Meola^{a,d,¹⁶}, P. Paolucci^{a,¹⁶}, C. Sciacca^{a,b}, E. Voevodina^{a,b}

INFN Sezione di Padova ^a, Università di Padova ^b, Padova, Italy, Università di Trento ^c, Trento, Italy

P. Azzi^a, N. Bacchetta^a, D. Bisello^{a,b}, A. Boletti^{a,b}, A. Bragagnolo, R. Carlin^{a,b}, P. Checchia^a, M. Dall'Osso^{a,b}, P. De Castro Manzano^a, T. Dorigo^a, U. Dosselli^a, F. Gasparini^{a,b}, U. Gasparini^{a,b}, A. Gozzelino^a, S.Y. Hoh, S. Lacaprara^a, P. Lujan, M. Margoni^{a,b}, A.T. Meneguzzo^{a,b}, J. Pazzini^{a,b}, M. Presilla^b, P. Ronchese^{a,b}, R. Rossin^{a,b}, F. Simonetto^{a,b}, A. Tiko, E. Torassa^a, M. Tosi^{a,b}, M. Zanetti^{a,b}, P. Zotto^{a,b}, G. Zumerle^{a,b}

INFN Sezione di Pavia ^a, Università di Pavia ^b, Pavia, Italy

A. Braghieri^a, A. Magnani^a, P. Montagna^{a,b}, S.P. Ratti^{a,b}, V. Re^a, M. Ressegotti^{a,b}, C. Riccardi^{a,b}, P. Salvini^a, I. Vai^{a,b}, P. Vitulo^{a,b}

INFN Sezione di Perugia ^a, Università di Perugia ^b, Perugia, Italy

M. Biasini^{a,b}, G.M. Bilei^a, C. Cecchi^{a,b}, D. Ciangottini^{a,b}, L. Fanò^{a,b}, P. Lariccia^{a,b}, R. Leonardi^{a,b}, E. Manoni^a, G. Mantovani^{a,b}, V. Mariani^{a,b}, M. Menichelli^a, A. Rossi^{a,b}, A. Santocchia^{a,b}, D. Spiga^a

INFN Sezione di Pisa ^a, Università di Pisa ^b, Scuola Normale Superiore di Pisa ^c, Pisa, Italy

K. Androsov^a, P. Azzurri^a, G. Bagliesi^a, L. Bianchini^a, T. Boccali^a, L. Borrello, R. Castaldi^a, M.A. Ciocci^{a,b}, R. Dell'Orso^a, G. Fedi^a, F. Fiori^{a,c}, L. Giannini^{a,c}, A. Giassi^a, M.T. Grippo^a, F. Ligabue^{a,c}, E. Manca^{a,c}, G. Mandorli^{a,c}, A. Messineo^{a,b}, F. Palla^a, A. Rizzi^{a,b}, G. Rolandi^{³¹}, P. Spagnolo^a, R. Tenchini^a, G. Tonelli^{a,b}, A. Venturi^a, P.G. Verdini^a

INFN Sezione di Roma ^a, Sapienza Università di Roma ^b, Rome, Italy

L. Barone^{a,b}, F. Cavallari^a, M. Cipriani^{a,b}, D. Del Re^{a,b}, E. Di Marco^{a,b}, M. Diemoz^a, S. Gelli^{a,b}, E. Longo^{a,b}, B. Marzocchi^{a,b}, P. Meridiani^a, G. Organtini^{a,b}, F. Pandolfi^a, R. Paramatti^{a,b}, F. Preiato^{a,b}, S. Rahatlou^{a,b}, C. Rovelli^a, F. Santanastasio^{a,b}

INFN Sezione di Torino ^a, Università di Torino ^b, Torino, Italy, Università del Piemonte Orientale ^c, Novara, Italy

N. Amapane^{a,b}, R. Arcidiacono^{a,c}, S. Argiro^{a,b}, M. Arneodo^{a,c}, N. Bartosik^a, R. Bellan^{a,b}, C. Biino^a, A. Cappati^{a,b}, N. Cartiglia^a, F. Cenna^{a,b}, S. Cometti^a, M. Costa^{a,b}, R. Covarelli^{a,b}, N. Demaria^a, B. Kiani^{a,b}, C. Mariotti^a, S. Maselli^a, E. Migliore^{a,b}, V. Monaco^{a,b}, E. Monteil^{a,b}, M. Monteno^a, M.M. Obertino^{a,b}, L. Pacher^{a,b}, N. Pastrone^a, M. Pelliccioni^a, G.L. Pinna Angioni^{a,b}, A. Romero^{a,b}, M. Ruspa^{a,c}, R. Sacchi^{a,b}, R. Salvatico^{a,b}, K. Shchelina^{a,b}, V. Sola^a, A. Solano^{a,b}, D. Soldi^{a,b}, A. Staiano^a

INFN Sezione di Trieste ^a, Università di Trieste ^b, Trieste, Italy

S. Belforte^a, V. Candelise^{a,b}, M. Casarsa^a, F. Cossutti^a, A. Da Rold^{a,b}, G. Della Ricca^{a,b}, F. Vazzoler^{a,b}, A. Zanetti^a

Kyungpook National University, Daegu, Korea

D.H. Kim, G.N. Kim, M.S. Kim, J. Lee, S. Lee, S.W. Lee, C.S. Moon, Y.D. Oh, S.I. Pak, S. Sekmen, D.C. Son, Y.C. Yang

Chonnam National University, Institute for Universe and Elementary Particles, Kwangju, Korea

H. Kim, D.H. Moon, G. Oh

Hanyang University, Seoul, Korea

B. Francois, J. Goh³², T.J. Kim

Korea University, Seoul, Korea

S. Cho, S. Choi, Y. Go, D. Gyun, S. Ha, B. Hong, Y. Jo, K. Lee, K.S. Lee, S. Lee, J. Lim, S.K. Park, Y. Roh

Sejong University, Seoul, Korea

H.S. Kim

Seoul National University, Seoul, Korea

J. Almond, J. Kim, J.S. Kim, H. Lee, K. Lee, K. Nam, S.B. Oh, B.C. Radburn-Smith, S.h. Seo, U.K. Yang, H.D. Yoo, G.B. Yu

University of Seoul, Seoul, Korea

D. Jeon, H. Kim, J.H. Kim, J.S.H. Lee, I.C. Park

Sungkyunkwan University, Suwon, Korea

Y. Choi, C. Hwang, J. Lee, I. Yu

Vilnius University, Vilnius, Lithuania

V. Dudenas, A. Juodagalvis, J. Vaitkus

National Centre for Particle Physics, Universiti Malaya, Kuala Lumpur, Malaysia

Z.A. Ibrahim, M.A.B. Md Ali³³, F. Mohamad Idris³⁴, W.A.T. Wan Abdullah, M.N. Yusli, Z. Zolkapli

Universidad de Sonora (UNISON), Hermosillo, Mexico

J.F. Benitez, A. Castaneda Hernandez, J.A. Murillo Quijada

Centro de Investigacion y de Estudios Avanzados del IPN, Mexico City, Mexico

H. Castilla-Valdez, E. De La Cruz-Burelo, M.C. Duran-Osuna, I. Heredia-De La Cruz³⁵, R. Lopez-Fernandez, J. Mejia Guisao, R.I. Rabadan-Trejo, M. Ramirez-Garcia, G. Ramirez-Sanchez, R. Reyes-Almanza, A. Sanchez-Hernandez

Universidad Iberoamericana, Mexico City, Mexico

S. Carrillo Moreno, C. Oropeza Barrera, F. Vazquez Valencia

Benemerita Universidad Autonoma de Puebla, Puebla, Mexico

J. Eysermans, I. Pedraza, H.A. Salazar Ibarguen, C. Uribe Estrada

Universidad Autónoma de San Luis Potosí, San Luis Potosí, Mexico

A. Morelos Pineda

University of Auckland, Auckland, New Zealand

D. Kofcheck

University of Canterbury, Christchurch, New Zealand

S. Bheesette, P.H. Butler

National Centre for Physics, Quaid-I-Azam University, Islamabad, Pakistan

A. Ahmad, M. Ahmad, M.I. Asghar, Q. Hassan, H.R. Hoorani, W.A. Khan, M.A. Shah, M. Shoaib, M. Waqas

National Centre for Nuclear Research, Swierk, Poland

H. Bialkowska, M. Bluj, B. Boimska, T. Frueboes, M. Górski, M. Kazana, M. Szleper, P. Traczyk, P. Zalewski

Institute of Experimental Physics, Faculty of Physics, University of Warsaw, Warsaw, Poland

K. Bunkowski, A. Byszuk³⁶, K. Doroba, A. Kalinowski, M. Konecki, J. Krolikowski, M. Misiura, M. Olszewski, A. Pyskir, M. Walczak

Laboratório de Instrumentação e Física Experimental de Partículas, Lisboa, Portugal

M. Araujo, P. Bargassa, C. Beirão Da Cruz E Silva, A. Di Francesco, P. Faccioli, B. Galinhas, M. Gallinaro, J. Hollar, N. Leonardo, J. Seixas, G. Strong, O. Toldaiev, J. Varela

Joint Institute for Nuclear Research, Dubna, Russia

S. Afanasiev, P. Bunin, M. Gavrilenko, I. Golutvin, I. Gorbunov, A. Kamenev, V. Karjiline, A. Lanev, A. Malakhov, V. Matveev^{37,38}, P. Moisenz, V. Palichik, V. Perelygin, S. Shmatov, S. Shulha, N. Skatchkov, V. Smirnov, N. Voytishin, A. Zarubin

Petersburg Nuclear Physics Institute, Gatchina (St. Petersburg), Russia

V. Golovtsov, Y. Ivanov, V. Kim³⁹, E. Kuznetsova⁴⁰, P. Levchenko, V. Murzin, V. Oreshkin, I. Smirnov, D. Sosnov, V. Sulimov, L. Uvarov, S. Vavilov, A. Vorobyev

Institute for Nuclear Research, Moscow, Russia

Yu. Andreev, A. Dermenev, S. Glinenko, N. Golubev, A. Karneyeu, M. Kirsanov, N. Krasnikov, A. Pashenkov, A. Shabanov, D. Tlisov, A. Toropin

Institute for Theoretical and Experimental Physics, Moscow, Russia

V. Epshteyn, V. Gavrilov, N. Lychkovskaya, V. Popov, I. Pozdnyakov, G. Safronov, A. Spiridonov, A. Stepenov, V. Stolin, M. Toms, E. Vlasov, A. Zhokin

Moscow Institute of Physics and Technology, Moscow, Russia

T. Aushev

National Research Nuclear University 'Moscow Engineering Physics Institute' (MEPhI), Moscow, Russia

R. Chistov⁴¹, M. Danilov⁴¹, S. Polikarpov⁴¹, E. Tarkovskii

P.N. Lebedev Physical Institute, Moscow, Russia

V. Andreev, M. Azarkin, I. Dremin³⁸, M. Kirakosyan, A. Terkulov

Skobeltsyn Institute of Nuclear Physics, Lomonosov Moscow State University, Moscow, Russia

A. Belyaev, E. Boos, V. Bunichev, M. Dubinin⁴², L. Dudko, A. Ershov, V. Klyukhin, O. Kodolova, I. Loktin, S. Obraztsov, M. Perfilov, V. Savrin, A. Snigirev

Novosibirsk State University (NSU), Novosibirsk, Russia

A. Barnyakov⁴³, V. Blinov⁴³, T. Dimova⁴³, L. Kardapoltsev⁴³, Y. Skovpen⁴³

Institute for High Energy Physics of National Research Centre 'Kurchatov Institute', Protvino, Russia

I. Azhgirey, I. Bayshev, S. Bitioukov, V. Kachanov, A. Kalinin, D. Konstantinov, P. Mandrik, V. Petrov, R. Ryutin, S. Slabospitskii, A. Sobol, S. Troshin, N. Tyurin, A. Uzunian, A. Volkov

National Research Tomsk Polytechnic University, Tomsk, Russia

A. Babaev, S. Baidali, V. Okhotnikov

University of Belgrade, Faculty of Physics and Vinca Institute of Nuclear Sciences, Belgrade, Serbia

P. Adzic⁴⁴, P. Cirkovic, D. Devetak, M. Dordevic, J. Milosevic

Centro de Investigaciones Energéticas Medioambientales y Tecnológicas (CIEMAT), Madrid, Spain

J. Alcaraz Maestre, A. Álvarez Fernández, I. Bachiller, M. Barrio Luna, J.A. Brochero Cifuentes, M. Cerrada, N. Colino, B. De La Cruz, A. Delgado Peris, C. Fernandez Bedoya, J.P. Fernández Ramos, J. Flix, M.C. Fouz, O. Gonzalez Lopez, S. Goy Lopez, J.M. Hernandez, M.I. Josa, D. Moran, A. Pérez-Calero Yzquierdo, J. Puerta Pelayo, I. Redondo, L. Romero, S. Sánchez Navas, M.S. Soares, A. Triossi

Universidad Autónoma de Madrid, Madrid, Spain

C. Albajar, J.F. de Trocóniz

Universidad de Oviedo, Oviedo, Spain

J. Cuevas, C. Erice, J. Fernandez Menendez, S. Folgueras, I. Gonzalez Caballero, J.R. González Fernández, E. Palencia Cortezon, V. Rodríguez Bouza, S. Sanchez Cruz, J.M. Vizan Garcia

Instituto de Física de Cantabria (IFCA), CSIC-Universidad de Cantabria, Santander, Spain

I.J. Cabrillo, A. Calderon, B. Chazin Quero, J. Duarte Campderros, M. Fernandez, P.J. Fernández Manteca, A. García Alonso, J. Garcia-Ferrero, G. Gomez, A. Lopez Virto, J. Marco, C. Martinez Rivero, P. Martinez Ruiz del Arbol, F. Matorras, J. Piedra Gomez, C. Prieels, T. Rodrigo, A. Ruiz-Jimeno, L. Scodellaro, N. Trevisani, I. Vila, R. Vilar Cortabitarte

University of Ruhuna, Department of Physics, Matara, Sri Lanka

N. Wickramage

CERN, European Organization for Nuclear Research, Geneva, Switzerland

D. Abbaneo, B. Akgun, E. Auffray, G. Auzinger, P. Baillon, A.H. Ball, D. Barney, J. Bendavid, M. Bianco, A. Bocci, C. Botta, E. Brondolin, T. Camporesi, M. Cepeda, G. Cerminara,

E. Chapon, Y. Chen, G. Cucciati, D. d'Enterria, A. Dabrowski, N. Daci, V. Daponte, A. David, A. De Roeck, N. Deelen, M. Dobson, M. Dünser, N. Dupont, A. Elliott-Peisert, P. Everaerts, F. Fallavollita⁴⁵, D. Fasanella, G. Franzoni, J. Fulcher, W. Funk, D. Gigi, A. Gilbert, K. Gill, F. Glege, M. Gruchala, M. Guilbaud, D. Gulhan, J. Hegeman, C. Heidegger, V. Innocente, A. Jafari, P. Janot, O. Karacheban¹⁹, J. Kieseler, A. Kornmayer, M. Krammer¹, C. Lange, P. Lecoq, C. Lourenço, L. Malgeri, M. Mannelli, A. Massironi, F. Meijers, J.A. Merlin, S. Mersi, E. Meschi, P. Milenovic⁴⁶, F. Moortgat, M. Mulders, J. Ngadiuba, S. Nourbakhsh, S. Orfanelli, L. Orsini, F. Pantaleo¹⁶, L. Pape, E. Perez, M. Peruzzi, A. Petrilli, G. Petrucciani, A. Pfeiffer, M. Pierini, F.M. Pitters, D. Rabady, A. Racz, T. Reis, M. Rovere, H. Sakulin, C. Schäfer, C. Schwick, M. Selvaggi, A. Sharma, P. Silva, P. Sphicas⁴⁷, A. Stakia, J. Steggemann, D. Treille, A. Tsirou, A. Vartak, V. Veckalns⁴⁸, M. Verzetti, W.D. Zeuner

Paul Scherrer Institut, Villigen, Switzerland

L. Caminada⁴⁹, K. Deiters, W. Erdmann, R. Horisberger, Q. Ingram, H.C. Kaestli, D. Kotlinski, U. Langenegger, T. Rohe, S.A. Wiederkehr

ETH Zurich - Institute for Particle Physics and Astrophysics (IPA), Zurich, Switzerland

M. Backhaus, L. Bäni, P. Berger, N. Chernyavskaya, G. Dissertori, M. Dittmar, M. Donegà, C. Dorfer, T.A. Gómez Espinosa, C. Grab, D. Hits, T. Klijnsma, W. Lustermann, R.A. Manzoni, M. Marionneau, M.T. Meinhard, F. Micheli, P. Musella, F. Nessi-Tedaldi, F. Pauss, G. Perrin, L. Perrozzi, S. Pigazzini, C. Reissel, D. Ruini, D.A. Sanz Becerra, M. Schönenberger, L. Shchutska, V.R. Tavolaro, K. Theofilatos, M.L. Vesterbacka Olsson, R. Wallny, D.H. Zhu

Universität Zürich, Zurich, Switzerland

T.K. Aarrestad, C. Amsler⁵⁰, D. Brzhechko, M.F. Canelli, A. De Cosa, R. Del Burgo, S. Donato, C. Galloni, T. Hreus, B. Kilminster, S. Leontsinis, I. Neutelings, G. Rauco, P. Robmann, D. Salerno, K. Schweiger, C. Seitz, Y. Takahashi, A. Zucchetta

National Central University, Chung-Li, Taiwan

T.H. Doan, R. Khurana, C.M. Kuo, W. Lin, A. Pozdnyakov, S.S. Yu

National Taiwan University (NTU), Taipei, Taiwan

P. Chang, Y. Chao, K.F. Chen, P.H. Chen, W.-S. Hou, Y.F. Liu, R.-S. Lu, E. Paganis, A. Psallidas, A. Steen

Chulalongkorn University, Faculty of Science, Department of Physics, Bangkok, Thailand

B. Asavapibhop, N. Srimanobhas, N. Suwonjandee

Çukurova University, Physics Department, Science and Art Faculty, Adana, Turkey

A. Bat, F. Boran, S. Cerci⁵¹, S. Damarseckin, Z.S. Demiroglu, F. Dolek, C. Dozen, I. Dumanoglu, G. Gokbulut, Y. Guler, E. Gurpinar, I. Hos⁵², C. Isik, E.E. Kangal⁵³, O. Kara, A. Kayis Topaksu, U. Kiminsu, M. Oglakci, G. Onengut, K. Ozdemir⁵⁴, S. Ozturk⁵⁵, D. Sunar Cerci⁵¹, B. Tali⁵¹, U.G. Tok, S. Turkcapar, I.S. Zorbakir, C. Zorbilmez

Middle East Technical University, Physics Department, Ankara, Turkey

B. Isildak⁵⁶, G. Karapinar⁵⁷, M. Yalvac, M. Zeyrek

Bogazici University, Istanbul, Turkey

I.O. Atakisi, E. Gülmез, M. Kaya⁵⁸, O. Kaya⁵⁹, S. Ozkorucuklu⁶⁰, S. Tekten, E.A. Yetkin⁶¹

Istanbul Technical University, Istanbul, Turkey

M.N. Agaras, A. Cakir, K. Cankocak, Y. Komurcu, S. Sen⁶²

Institute for Scintillation Materials of National Academy of Science of Ukraine, Kharkov, Ukraine

B. Grynyov

National Scientific Center, Kharkov Institute of Physics and Technology, Kharkov, Ukraine

L. Levchuk

University of Bristol, Bristol, United Kingdom

F. Ball, J.J. Brooke, D. Burns, E. Clement, D. Cussans, O. Davignon, H. Flacher, J. Goldstein, G.P. Heath, H.F. Heath, L. Kreczko, D.M. Newbold⁶³, S. Paramesvaran, B. Penning, T. Sakuma, D. Smith, V.J. Smith, J. Taylor, A. Titterton

Rutherford Appleton Laboratory, Didcot, United Kingdom

K.W. Bell, A. Belyaev⁶⁴, C. Brew, R.M. Brown, D. Cieri, D.J.A. Cockerill, J.A. Coughlan, K. Harder, S. Harper, J. Linacre, K. Manolopoulos, E. Olaiya, D. Petyt, C.H. Shepherd-Themistocleous, A. Thea, I.R. Tomalin, T. Williams, W.J. Womersley

Imperial College, London, United Kingdom

R. Bainbridge, P. Bloch, J. Borg, S. Breeze, O. Buchmuller, A. Bundock, D. Colling, P. Dauncey, G. Davies, M. Della Negra, R. Di Maria, G. Hall, G. Iles, T. James, M. Komm, C. Laner, L. Lyons, A.-M. Magnan, S. Malik, A. Martelli, J. Nash⁶⁵, A. Nikitenko⁷, V. Palladino, M. Pesaresi, D.M. Raymond, A. Richards, A. Rose, E. Scott, C. Seez, A. Shtipliyski, G. Singh, M. Stoye, T. Strebler, S. Summers, A. Tapper, K. Uchida, T. Virdee¹⁶, N. Wardle, D. Winterbottom, J. Wright, S.C. Zenz

Brunel University, Uxbridge, United Kingdom

J.E. Cole, P.R. Hobson, A. Khan, P. Kyberd, C.K. Mackay, A. Morton, I.D. Reid, L. Teodorescu, S. Zahid

Baylor University, Waco, USA

K. Call, J. Dittmann, K. Hatakeyama, H. Liu, C. Madrid, B. McMaster, N. Pastika, C. Smith

Catholic University of America, Washington, DC, USA

R. Bartek, A. Dominguez

The University of Alabama, Tuscaloosa, USA

A. Buccilli, S.I. Cooper, C. Henderson, P. Rumerio, C. West

Boston University, Boston, USA

D. Arcaro, T. Bose, D. Gastler, S. Giris, D. Pinna, C. Richardson, J. Rohlf, L. Sulak, D. Zou

Brown University, Providence, USA

G. Benelli, B. Burkle, X. Coubez, D. Cutts, M. Hadley, J. Hakala, U. Heintz, J.M. Hogan⁶⁶, K.H.M. Kwok, E. Laird, G. Landsberg, J. Lee, Z. Mao, M. Narain, S. Sagir⁶⁷, R. Syarif, E. Usai, D. Yu

University of California, Davis, Davis, USA

R. Band, C. Brainerd, R. Breedon, D. Burns, M. Calderon De La Barca Sanchez, M. Chertok, J. Conway, R. Conway, P.T. Cox, R. Erbacher, C. Flores, G. Funk, W. Ko, O. Kukral, R. Lander, M. Mulhearn, D. Pellett, J. Pilot, S. Shalhout, M. Shi, D. Stolp, D. Taylor, K. Tos, M. Tripathi, Z. Wang, F. Zhang

University of California, Los Angeles, USA

M. Bachtis, C. Bravo, R. Cousins, A. Dasgupta, S. Erhan, A. Florent, J. Hauser, M. Ignatenko, N. Mccoll, S. Regnard, D. Saltzberg, C. Schnaible, V. Valuev

University of California, Riverside, Riverside, USA

E. Bouvier, K. Burt, R. Clare, J.W. Gary, S.M.A. Ghiasi Shirazi, G. Hanson, G. Karapostoli, E. Kennedy, F. Lacroix, O.R. Long, M. Olmedo Negrete, M.I. Paneva, W. Si, L. Wang, H. Wei, S. Wimpenny, B.R. Yates

University of California, San Diego, La Jolla, USA

J.G. Branson, P. Chang, S. Cittolin, M. Derdzinski, R. Gerosa, D. Gilbert, B. Hashemi, A. Holzner, D. Klein, G. Kole, V. Krutelyov, J. Letts, M. Masciovecchio, S. May, D. Olivito, S. Padhi, M. Pieri, V. Sharma, M. Tadel, J. Wood, F. Würthwein, A. Yagil, G. Zevi Della Porta

University of California, Santa Barbara - Department of Physics, Santa Barbara, USA

N. Amin, R. Bhandari, C. Campagnari, M. Citron, V. Dutta, M. Franco Sevilla, L. Gouskos, R. Heller, J. Incandela, H. Mei, A. Ovcharova, H. Qu, J. Richman, D. Stuart, I. Suarez, S. Wang, J. Yoo

California Institute of Technology, Pasadena, USA

D. Anderson, A. Bornheim, J.M. Lawhorn, N. Lu, H.B. Newman, T.Q. Nguyen, J. Pata, M. Spiropulu, J.R. Vlimant, R. Wilkinson, S. Xie, Z. Zhang, R.Y. Zhu

Carnegie Mellon University, Pittsburgh, USA

M.B. Andrews, T. Ferguson, T. Mudholkar, M. Paulini, M. Sun, I. Vorobiev, M. Weinberg

University of Colorado Boulder, Boulder, USA

J.P. Cumalat, W.T. Ford, F. Jensen, A. Johnson, E. MacDonald, T. Mulholland, R. Patel, A. Perloff, K. Stenson, K.A. Ulmer, S.R. Wagner

Cornell University, Ithaca, USA

J. Alexander, J. Chaves, Y. Cheng, J. Chu, A. Datta, K. Mcdermott, N. Mirman, J.R. Patterson, D. Quach, A. Rinkevicius, A. Ryd, L. Skinnari, L. Soffi, S.M. Tan, Z. Tao, J. Thom, J. Tucker, P. Wittich, M. Zientek

Fermi National Accelerator Laboratory, Batavia, USA

S. Abdullin, M. Albrow, M. Alyari, G. Apollinari, A. Apresyan, A. Apyan, S. Banerjee, L.A.T. Bauerdtick, A. Beretvas, J. Berryhill, P.C. Bhat, K. Burkett, J.N. Butler, A. Canepa, G.B. Cerati, H.W.K. Cheung, F. Chlebana, M. Cremonesi, J. Duarte, V.D. Elvira, J. Freeman, Z. Gecse, E. Gottschalk, L. Gray, D. Green, S. Grünendahl, O. Gutsche, J. Hanlon, R.M. Harris, S. Hasegawa, J. Hirschauer, Z. Hu, B. Jayatilaka, S. Jindariani, M. Johnson, U. Joshi, B. Klima, M.J. Kortelainen, B. Kreis, S. Lammel, D. Lincoln, R. Lipton, M. Liu, T. Liu, J. Lykken, K. Maeshima, J.M. Marraffino, D. Mason, P. McBride, P. Merkel, S. Mrenna, S. Nahn, V. O'Dell, K. Pedro, C. Pena, O. Prokofyev, G. Rakness, F. Ravera, A. Reinsvold, L. Ristori, A. Savoy-Navarro⁶⁸, B. Schneider, E. Sexton-Kennedy, A. Soha, W.J. Spalding, L. Spiegel, S. Stoynev, J. Strait, N. Strobbe, L. Taylor, S. Tkaczyk, N.V. Tran, L. Uplegger, E.W. Vaandering, C. Vernieri, M. Verzocchi, R. Vidal, M. Wang, H.A. Weber

University of Florida, Gainesville, USA

D. Acosta, P. Avery, P. Bortignon, D. Bourilkov, A. Brinkerhoff, L. Cadamuro, A. Carnes, D. Curry, R.D. Field, S.V. Gleyzer, B.M. Joshi, J. Konigsberg, A. Korytov, K.H. Lo, P. Ma, K. Matchev, G. Mitselmakher, D. Rosenzweig, K. Shi, D. Sperka, J. Wang, S. Wang, X. Zuo

Florida International University, Miami, USA

Y.R. Joshi, S. Linn

Florida State University, Tallahassee, USA

A. Ackert, T. Adams, A. Askew, S. Hagopian, V. Hagopian, K.F. Johnson, T. Kolberg, G. Martinez, T. Perry, H. Prosper, A. Saha, C. Schiber, R. Yohay

Florida Institute of Technology, Melbourne, USA

M.M. Baarmann, V. Bhopatkar, S. Colafranceschi, M. Hohlmann, D. Noonan, M. Rahmani, T. Roy, M. Saunders, F. Yumiceva

University of Illinois at Chicago (UIC), Chicago, USA

M.R. Adams, L. Apanasevich, D. Berry, R.R. Betts, R. Cavanaugh, X. Chen, S. Dittmer, O. Evdokimov, C.E. Gerber, D.A. Hangal, D.J. Hofman, K. Jung, J. Kamin, C. Mills, M.B. Tonjes, N. Varelas, H. Wang, X. Wang, Z. Wu, J. Zhang

The University of Iowa, Iowa City, USA

M. Alhusseini, B. Bilki⁶⁹, W. Clarida, K. Dilsiz⁷⁰, S. Durgut, R.P. Gandrajula, M. Haytmyradov, V. Khristenko, J.-P. Merlo, A. Mestvirishvili, A. Moeller, J. Nachtman, H. Ogul⁷¹, Y. Onel, F. Ozok⁷², A. Penzo, C. Snyder, E. Tiras, J. Wetzel

Johns Hopkins University, Baltimore, USA

B. Blumenfeld, A. Cocoros, N. Eminizer, D. Fehling, L. Feng, A.V. Gritsan, W.T. Hung, P. Maksimovic, J. Roskes, U. Sarica, M. Swartz, M. Xiao

The University of Kansas, Lawrence, USA

A. Al-bataineh, P. Baringer, A. Bean, S. Boren, J. Bowen, A. Bylinkin, J. Castle, S. Khalil, A. Kropivnitskaya, D. Majumder, W. Mcbrayer, M. Murray, C. Rogan, S. Sanders, E. Schmitz, J.D. Tapia Takaki, Q. Wang

Kansas State University, Manhattan, USA

S. Duric, A. Ivanov, K. Kaadze, D. Kim, Y. Maravin, D.R. Mendis, T. Mitchell, A. Modak, A. Mohammadi

Lawrence Livermore National Laboratory, Livermore, USA

F. Rebassoo, D. Wright

University of Maryland, College Park, USA

A. Baden, O. Baron, A. Belloni, S.C. Eno, Y. Feng, C. Ferraioli, N.J. Hadley, S. Jabeen, G.Y. Jeng, R.G. Kellogg, J. Kunkle, A.C. Mignerey, S. Nabili, F. Ricci-Tam, M. Seidel, Y.H. Shin, A. Skuja, S.C. Tonwar, K. Wong

Massachusetts Institute of Technology, Cambridge, USA

D. Abercrombie, B. Allen, V. Azzolini, A. Baty, R. Bi, S. Brandt, W. Busza, I.A. Cali, M. D'Alfonso, Z. Demiragli, G. Gomez Ceballos, M. Goncharov, P. Harris, D. Hsu, M. Hu, Y. Iiyama, G.M. Innocenti, M. Klute, D. Kovalevsky, Y.-J. Lee, P.D. Luckey, B. Maier, A.C. Marini, C. McGinn, C. Mironov, S. Narayanan, X. Niu, C. Paus, D. Rankin, C. Roland, G. Roland, Z. Shi, G.S.F. Stephans, K. Sumorok, K. Tatar, D. Velicanu, J. Wang, T.W. Wang, B. Wyslouch

University of Minnesota, Minneapolis, USA

A.C. Benvenuti[†], R.M. Chatterjee, A. Evans, P. Hansen, J. Hiltbrand, Sh. Jain, S. Kalafut, M. Krohn, Y. Kubota, Z. Lesko, J. Mans, R. Rusack, M.A. Wadud

University of Mississippi, Oxford, USA

J.G. Acosta, S. Oliveros

University of Nebraska-Lincoln, Lincoln, USA

E. Avdeeva, K. Bloom, D.R. Claes, C. Fangmeier, F. Golf, R. Gonzalez Suarez, R. Kamalieddin, I. Kravchenko, J. Monroy, J.E. Siado, G.R. Snow, B. Stieger

State University of New York at Buffalo, Buffalo, USA

A. Godshalk, C. Harrington, I. Iashvili, A. Kharchilava, C. Mclean, D. Nguyen, A. Parker, S. Rappoccio, B. Roozbahani

Northeastern University, Boston, USA

G. Alverson, E. Barberis, C. Freer, Y. Haddad, A. Hortiangtham, G. Madigan, D.M. Morse, T. Orimoto, A. Tishelman-charny, T. Wamorkar, B. Wang, A. Wisecarver, D. Wood

Northwestern University, Evanston, USA

S. Bhattacharya, J. Bueghly, O. Charaf, T. Gunter, K.A. Hahn, N. Odell, M.H. Schmitt, K. Sung, M. Trovato, M. Velasco

University of Notre Dame, Notre Dame, USA

R. Bucci, N. Dev, R. Goldouzian, M. Hildreth, K. Hurtado Anampa, C. Jessop, D.J. Karmgard, K. Lannon, W. Li, N. Loukas, N. Marinelli, F. Meng, C. Mueller, Y. Musienko³⁷, M. Planer, R. Ruchti, P. Siddireddy, G. Smith, S. Taroni, M. Wayne, A. Wightman, M. Wolf, A. Woodard

The Ohio State University, Columbus, USA

J. Alimena, L. Antonelli, B. Bylsma, L.S. Durkin, S. Flowers, B. Francis, C. Hill, W. Ji, T.Y. Ling, W. Luo, B.L. Winer

Princeton University, Princeton, USA

S. Cooperstein, P. Elmer, J. Hardenbrook, N. Haubrich, S. Higginbotham, A. Kalogeropoulos, S. Kwan, D. Lange, M.T. Lucchini, J. Luo, D. Marlow, K. Mei, I. Ojalvo, J. Olsen, C. Palmer, P. Piroué, J. Salfeld-Nebgen, D. Stickland, C. Tully

University of Puerto Rico, Mayaguez, USA

S. Malik, S. Norberg

Purdue University, West Lafayette, USA

A. Barker, V.E. Barnes, S. Das, L. Gutay, M. Jones, A.W. Jung, A. Khatiwada, B. Mahakud, D.H. Miller, N. Neumeister, C.C. Peng, S. Piperov, H. Qiu, J.F. Schulte, J. Sun, F. Wang, R. Xiao, W. Xie

Purdue University Northwest, Hammond, USA

T. Cheng, J. Dolen, N. Parashar

Rice University, Houston, USA

Z. Chen, K.M. Ecklund, S. Freed, F.J.M. Geurts, M. Kilpatrick, Arun Kumar, W. Li, B.P. Padley, R. Redjimi, J. Roberts, J. Rorie, W. Shi, Z. Tu, A. Zhang

University of Rochester, Rochester, USA

A. Bodek, P. de Barbaro, R. Demina, Y.t. Duh, J.L. Dulemba, C. Fallon, T. Ferbel, M. Galanti, A. Garcia-Bellido, J. Han, O. Hindrichs, A. Khukhunaishvili, E. Ranken, P. Tan, R. Taus

Rutgers, The State University of New Jersey, Piscataway, USA

B. Chiarito, J.P. Chou, Y. Gershtein, E. Halkiadakis, A. Hart, M. Heindl, E. Hughes, S. Kaplan, R. Kuninawalkam Elayavalli, S. Kyriacou, I. Laflotte, A. Lath, R. Montalvo, K. Nash, M. Osherson, H. Saka, S. Salur, S. Schnetzer, D. Sheffield, S. Somalwar, R. Stone, S. Thomas, P. Thomassen

University of Tennessee, Knoxville, USA

H. Acharya, A.G. Delannoy, J. Heideman, G. Riley, S. Spanier

Texas A&M University, College Station, USA

O. Bouhali⁷³, A. Celik, M. Dalchenko, M. De Mattia, A. Delgado, S. Dildick, R. Eusebi,

J. Gilmore, T. Huang, T. Kamon⁷⁴, S. Luo, D. Marley, R. Mueller, D. Overton, L. Perniè, D. Rathjens, A. Safonov

Texas Tech University, Lubbock, USA

N. Akchurin, J. Damgov, F. De Guio, P.R. Dudero, S. Kunori, K. Lamichhane, S.W. Lee, T. Mengke, S. Muthumuni, T. Peltola, S. Undleeb, I. Volobouev, Z. Wang, A. Whitbeck

Vanderbilt University, Nashville, USA

S. Greene, A. Gurrola, R. Janjam, W. Johns, C. Maguire, A. Melo, H. Ni, K. Padeken, F. Romeo, J.D. Ruiz Alvarez, P. Sheldon, S. Tuo, J. Velkovska, M. Verweij, Q. Xu

University of Virginia, Charlottesville, USA

M.W. Arenton, P. Barria, B. Cox, R. Hirosky, M. Joyce, A. Ledovskoy, H. Li, C. Neu, T. Sinthuprasith, Y. Wang, E. Wolfe, F. Xia

Wayne State University, Detroit, USA

R. Harr, P.E. Karchin, N. Poudyal, J. Sturdy, P. Thapa, S. Zaleski

University of Wisconsin - Madison, Madison, WI, USA

J. Buchanan, C. Caillol, D. Carlsmith, S. Dasu, I. De Bruyn, L. Dodd, B. Gomber⁷⁵, M. Grothe, M. Herndon, A. Hervé, U. Hussain, P. Klabbers, A. Lanaro, K. Long, R. Loveless, T. Ruggles, A. Savin, V. Sharma, N. Smith, W.H. Smith, N. Woods

†: Deceased

- 1: Also at Vienna University of Technology, Vienna, Austria
- 2: Also at IRFU, CEA, Université Paris-Saclay, Gif-sur-Yvette, France
- 3: Also at Universidade Estadual de Campinas, Campinas, Brazil
- 4: Also at Federal University of Rio Grande do Sul, Porto Alegre, Brazil
- 5: Also at Université Libre de Bruxelles, Bruxelles, Belgium
- 6: Also at University of Chinese Academy of Sciences, Beijing, China
- 7: Also at Institute for Theoretical and Experimental Physics, Moscow, Russia
- 8: Also at Joint Institute for Nuclear Research, Dubna, Russia
- 9: Now at British University in Egypt, Cairo, Egypt
- 10: Now at Helwan University, Cairo, Egypt
- 11: Now at Fayoum University, El-Fayoum, Egypt
- 12: Also at Department of Physics, King Abdulaziz University, Jeddah, Saudi Arabia
- 13: Also at Université de Haute Alsace, Mulhouse, France
- 14: Also at Skobeltsyn Institute of Nuclear Physics, Lomonosov Moscow State University, Moscow, Russia
- 15: Also at Tbilisi State University, Tbilisi, Georgia
- 16: Also at CERN, European Organization for Nuclear Research, Geneva, Switzerland
- 17: Also at RWTH Aachen University, III. Physikalisches Institut A, Aachen, Germany
- 18: Also at University of Hamburg, Hamburg, Germany
- 19: Also at Brandenburg University of Technology, Cottbus, Germany
- 20: Also at Institute of Physics, University of Debrecen, Debrecen, Hungary
- 21: Also at Institute of Nuclear Research ATOMKI, Debrecen, Hungary
- 22: Also at MTA-ELTE Lendület CMS Particle and Nuclear Physics Group, Eötvös Loránd University, Budapest, Hungary
- 23: Also at Indian Institute of Technology Bhubaneswar, Bhubaneswar, India
- 24: Also at Institute of Physics, Bhubaneswar, India
- 25: Also at Shoolini University, Solan, India
- 26: Also at University of Visva-Bharati, Santiniketan, India

- 27: Also at Isfahan University of Technology, Isfahan, Iran
28: Also at Plasma Physics Research Center, Science and Research Branch, Islamic Azad University, Tehran, Iran
29: Also at ITALIAN NATIONAL AGENCY FOR NEW TECHNOLOGIES, ENERGY AND SUSTAINABLE ECONOMIC DEVELOPMENT, Bologna, Italy
30: Also at Università degli Studi di Siena, Siena, Italy
31: Also at Scuola Normale e Sezione dell'INFN, Pisa, Italy
32: Also at Kyunghee University, Seoul, Korea
33: Also at International Islamic University of Malaysia, Kuala Lumpur, Malaysia
34: Also at Malaysian Nuclear Agency, MOSTI, Kajang, Malaysia
35: Also at Consejo Nacional de Ciencia y Tecnología, Mexico City, Mexico
36: Also at Warsaw University of Technology, Institute of Electronic Systems, Warsaw, Poland
37: Also at Institute for Nuclear Research, Moscow, Russia
38: Now at National Research Nuclear University 'Moscow Engineering Physics Institute' (MEPhI), Moscow, Russia
39: Also at St. Petersburg State Polytechnical University, St. Petersburg, Russia
40: Also at University of Florida, Gainesville, USA
41: Also at P.N. Lebedev Physical Institute, Moscow, Russia
42: Also at California Institute of Technology, Pasadena, USA
43: Also at Budker Institute of Nuclear Physics, Novosibirsk, Russia
44: Also at Faculty of Physics, University of Belgrade, Belgrade, Serbia
45: Also at INFN Sezione di Pavia ^a, Università di Pavia ^b, Pavia, Italy
46: Also at University of Belgrade, Faculty of Physics and Vinca Institute of Nuclear Sciences, Belgrade, Serbia
47: Also at National and Kapodistrian University of Athens, Athens, Greece
48: Also at Riga Technical University, Riga, Latvia
49: Also at Universität Zürich, Zurich, Switzerland
50: Also at Stefan Meyer Institute for Subatomic Physics (SMI), Vienna, Austria
51: Also at Adiyaman University, Adiyaman, Turkey
52: Also at Istanbul Aydin University, Istanbul, Turkey
53: Also at Mersin University, Mersin, Turkey
54: Also at Piri Reis University, Istanbul, Turkey
55: Also at Gaziosmanpasa University, Tokat, Turkey
56: Also at Ozyegin University, Istanbul, Turkey
57: Also at Izmir Institute of Technology, Izmir, Turkey
58: Also at Marmara University, Istanbul, Turkey
59: Also at Kafkas University, Kars, Turkey
60: Also at Istanbul University, Faculty of Science, Istanbul, Turkey
61: Also at Istanbul Bilgi University, Istanbul, Turkey
62: Also at Hacettepe University, Ankara, Turkey
63: Also at Rutherford Appleton Laboratory, Didcot, United Kingdom
64: Also at School of Physics and Astronomy, University of Southampton, Southampton, United Kingdom
65: Also at Monash University, Faculty of Science, Clayton, Australia
66: Also at Bethel University, St. Paul, USA
67: Also at Karamanoğlu Mehmetbey University, Karaman, Turkey
68: Also at Purdue University, West Lafayette, USA
69: Also at Beykent University, Istanbul, Turkey
70: Also at Bingol University, Bingol, Turkey

- 71: Also at Sinop University, Sinop, Turkey
- 72: Also at Mimar Sinan University, Istanbul, Istanbul, Turkey
- 73: Also at Texas A&M University at Qatar, Doha, Qatar
- 74: Also at Kyungpook National University, Daegu, Korea
- 75: Also at University of Hyderabad, Hyderabad, India